NASA/TM-20240016491/CORRECTED

GVIPS Prediction of Cyclic Ratchetting Behavior and Cycles with Interrupted Relaxation Periods of TIMETAL 21S at 650 °C

Steven M. Arnold
Glenn Research Center, Cleveland, Ohio

Paria Naghipour Ghezeljeh
Ohio Aerospace Institute, Brook Park, Ohio

Cliff J. Lissenden
Penn State University, University Park, Pennsylvania

Corrected Copy issued April 2026.

December 2024

NASA STI Program Report Series

Since its founding, NASA has been dedicated to the advancement of aeronautics and space science. The NASA scientific and technical information (STI) program plays a key part in helping NASA maintain this important role.

The NASA STI program operates under the auspices of the Agency Chief Information Officer. It collects, organizes, provides for archiving, and disseminates NASA's STI. The NASA STI program provides access to the NTRS Registered and its public interface, the NASA Technical Reports Server, thus providing one of the largest collections of aeronautical and space science STI in the world. Results are published in both non-NASA channels and by NASA in the NASA STI Report Series, which includes the following report types:

- TECHNICAL PUBLICATION.
  Reports of completed research or a major significant phase of research that present the results of NASA programs and include extensive data or theoretical analysis. Includes compilations of significant scientific and technical data and information deemed to be of continuing reference value. NASA counterpart of peer-reviewed formal professional papers but has less stringent limitations on manuscript length and extent of graphic presentations.

- TECHNICAL MEMORANDUM.
  Scientific and technical findings that are preliminary or of specialized interest, e.g., quick release reports, working papers, and bibliographies that contain minimal annotation. Does not contain extensive analysis.

- CONTRACTOR REPORT.
  Scientific and technical findings by NASA-sponsored contractors and grantees.

- CONFERENCE PUBLICATION.
  Collected papers from scientific and technical conferences, symposia, seminars, or other meetings sponsored or cosponsored by NASA.

- SPECIAL PUBLICATION.
  Scientific, technical, or historical information from NASA programs, projects, and missions, often concerned with subjects having substantial public interest.

- TECHNICAL TRANSLATION.
  English-language translations of foreign scientific and technical material pertinent to NASA's mission.

Specialized services also include organizing and publishing research results, distributing specialized research announcements and feeds, providing information desk and personal search support, and enabling data exchange services.

For more information about the NASA STI program, see the following:

- Access the NASA STI program home page at http://www.sti.nasa.gov

NASA/TM-20240016491/CORRECTED

GVIPS Prediction of Cyclic Ratchetting Behavior and Cycles with Interrupted Relaxation Periods of TIMETAL 21S at 650 °C

Steven M. Arnold
Glenn Research Center, Cleveland, Ohio

Paria Naghipour Ghezeljeh
Ohio Aerospace Institute, Brook Park, Ohio

Cliff J. Lissenden
Penn State University, University Park, Pennsylvania

Corrected Copy issued April 2026.

National Aeronautics and
Space Administration

Glenn Research Center
Cleveland, Ohio 44135

December 2024

Acknowledgments

Authors would like to thank the Transformational Tools and Technology (TTT) project for funding this work.

Level of Review: This material has been technically reviewed by technical management.

This report is available in electronic form at https://www.sti.nasa.gov/ and https://ntrs.nasa.gov/

NASA STI Program/Mail Stop 050
NASA Langley Research Center
Hampton, VA 23681-2199

Corrected Copy

Issued April 2026 for

NASA/TM-20240016491

GVIPS Prediction of Cyclic Ratchetting Behavior and Cycles with Interrupted Relaxation Periods of TIMETAL 21S at 650 °C

Steven M. Arnold, Paria Naghipour Ghezeljeh, and Cliff J. Lissenden

December 2024

Eight equations were corrected:

(1) Page 3: Equation (4) was corrected to change Ω_R to Φ_R.

Original: $$\varepsilon_{ij} - \varepsilon_{ij}^{vp} = \frac{\partial \Omega_R}{\partial (\sigma_s)_{ij}}$$

Corrected: $$\varepsilon_{ij} - \varepsilon_{ij}^{vp} = \frac{\partial \Phi_R}{\partial (\sigma_s)_{ij}}$$

(2) Page 3: Equation (5) was corrected to change Ω_R to Φ_R and $-p_{ij}^{(a)}$ was removed.

Original: $$\varepsilon_{ij}^{ve} - p_{ij}^{(a)} = \frac{\partial \Omega_R}{\partial q_{ij}^{(a)}}$$

Corrected: $$\varepsilon_{ij}^{ve} = \frac{\partial \Phi_R}{\partial q_{ij}^{(a)}}$$

(3) Page 3: Equation (6) was corrected to change Ω_{IR} to $\phi\Phi_{IR}$.

Original: $$\gamma_{ij}^{(b)} = \frac{\partial \Omega_{IR}}{\partial \alpha_{ij}^{(b)}}$$

Corrected: $$\gamma_{ij}^{(b)} = \frac{\partial \Phi_{IR}}{\partial \alpha_{ij}^{(b)}}$$

(4) Page 4: Equation (7) was corrected to change Ω_R to Φ_R.

Original: $$\dot{\varepsilon}_{ij} - \dot{\varepsilon}_{ij}^{vp} = \frac{\mathrm{d}}{\mathrm{d}t}\frac{\partial \Omega_R}{\partial (\sigma_s)_{ij}} = \frac{\partial^2 \Omega_R}{\partial (\sigma_s)_{ij}\, \partial (\sigma_s)_{kl}} (\dot{\sigma}_s)_{kl}$$

Corrected: $$\dot{\varepsilon}_{ij} - \dot{\varepsilon}_{ij}^{vp} = \frac{\mathrm{d}}{\mathrm{d}t}\frac{\partial \Phi_R}{\partial (\sigma_s)_{ij}} = \frac{\partial^2 \Phi_R}{\partial (\sigma_s)_{ij}\, \partial (\sigma_s)_{kl}} (\dot{\sigma}_s)_{kl}$$

(5) Page 4: Equation (8) was corrected to change Ω_R to Φ_R and $-p_{ij}^{(a)}$ was removed.

Original: $$\dot{\varepsilon}_{ij}^{ve} - p_{ij}^{(a)} = \frac{\mathrm{d}}{\mathrm{d}t}\frac{\partial \Omega_R}{\partial q_{ij}^{(a)}} = \frac{\partial^2 \Omega_R}{\partial q_{ij}^{(a)} \partial q_{kl}^{(a)}} \dot{q}_{kl}^{(a)}$$

Corrected: $$\dot{\varepsilon}_{ij}^{ve} = \frac{\mathrm{d}}{\mathrm{d}t}\frac{\partial \Phi_R}{\partial q_{ij}^{(a)}} = \frac{\partial^2 \Phi_R}{\partial q_{ij}^{(a)} \partial q_{kl}^{(a)}} \dot{q}_{kl}^{(a)}$$

(6) Page 4: Equation (9) was corrected to change Ω_{IR} to Φ_{IR}.

Original: $$\dot{\gamma}_{ij}^{(b)} = \frac{\mathrm{d}}{\mathrm{d}t}\frac{\partial \Omega_{IR}}{\partial \alpha_{ij}^{(b)}} = \frac{\partial^2 \Omega_{IR}}{\partial \alpha_{ij}^{(b)} \partial \alpha_{kl}^{(b)}} \dot{\alpha}_{kl}^{(b)} \quad \text{or} \quad \dot{\alpha}_{kl}^{(b)} = \left[\frac{\partial^2 \Omega_{IR}}{\partial \alpha_{ij}^{(b)} \partial \alpha_{kl}^{(b)}} \right]^{-1} \dot{\gamma}_{ij}^{(b)}$$

Corrected: $$\dot{\gamma}_{ij}^{(b)} = \frac{\mathrm{d}}{\mathrm{d}t}\frac{\partial \Phi_{IR}}{\partial \alpha_{ij}^{(b)}} = \frac{\partial^2 \Phi_{IR}}{\partial \alpha_{ij}^{(b)} \partial \alpha_{kl}^{(b)}} \dot{\alpha}_{kl}^{(b)} \quad \text{or} \quad \dot{\alpha}_{kl}^{(b)} = \left[\frac{\partial^2 \Phi_{IR}}{\partial \alpha_{ij}^{(b)} \partial \alpha_{kl}^{(b)}} \right]^{-1} \dot{\gamma}_{ij}^{(b)}$$

(7) Page 5: Equation (18) was corrected to remove 1/2.

Original: $$\Omega_{IR} = \Omega_1(F) + \frac{1}{2}\sum_{b=1}^{N} \Omega_2^{(b)}\left(G^{(b)}\right)$$

Corrected: $$\Omega_{IR} = \Omega_1(F) + \sum_{b=1}^{N} \Omega_2^{(b)}\left(G^{(b)}\right)$$

(8) Page 7: Equation (25) was corrected to change the plus sign to a minus sign.

Original: $$\dot{q}_{ij}^{(a)} = M_{ijkl}\left(\dot{\varepsilon}_{kl} - \dot{\varepsilon}_{kl}^{vp}\right) + M_{ijkl}\eta_{klrs}^{-1}\dot{q}_{rs}^{(a)}$$

Corrected: $$\dot{q}_{ij}^{(a)} = M_{ijkl}\left(\dot{\varepsilon}_{kl} - \dot{\varepsilon}_{kl}^{vp}\right) - M_{ijkl}\eta_{klrs}^{-1}\dot{q}_{rs}^{(a)}$$

(9) Page 7: Equation (29) was corrected to remove the prime.

Original: $$h'(\cdot) = \frac{1}{k_{(b)}^2}\frac{\partial h'(\cdot)}{\partial G^{(b)}}$$

Corrected: $$h'(\cdot) = \frac{1}{k_{(b)}^2}\frac{\partial h(\cdot)}{\partial G^{(b)}}$$

GVIPS Prediction of Cyclic Ratchetting Behavior and Cycles with Interrupted Relaxation Periods of TIMETAL 21S at 650 °C

Steven M. Arnold
National Aeronautics and Space Administration
Glenn Research Center
Cleveland, Ohio 44135

Paria Naghipour Ghezeljeh
HX5, LLC
Brook Park, Ohio 44142

Cliff J. Lissenden
Penn State University
University Park, Pennsylvania 16802

Abstract

The predictive performance of a multimechanism GVIPS model with saturating hardening function is assessed against a set of high temperature cyclic experiments under both strain-control and stress-control at varying rates of loading as well as several complex interrupted cyclic responses. The material specimens were composed of the titanium alloy, TIMETAL 21S, and tested at 650 °C, see Lissenden et al., 2007. The model did a very good job of predicting the variety of tests, particularly given the fact that only monotonic loading tests (tensile, creep, relaxation) and a single fully reversed cycle was used for characterization. It was particularly interesting that the model was capable of reasonably capturing the rate of accumulated strain during ratchetting under tensile mean stress. Given complex interrupted cyclic response, the model was able to both qualitatively and even quantitatively predict reasonably well both the cyclic and associated relaxation periods (in all quadrants of the stress-strain space) thus confirming the validity of the chosen functional forms for both hardening and thermal recovery. The quantitative inaccuracy is associated with the fact that the material specimens tested by Lissenden et al., 2007 was significantly "softer" than those tested by Castelli in Saleeb et al., 1994 which were used for characterization of the GVIPS model parameters.

Introduction

Extensive research efforts have been made over the years on the phenomenological representations of material behavior. Significant progress has been made in the development of theories of viscoelasticity and viscoplasticity for the modeling of inelastic properties. In particular, the present state-of-the-art in mathematical modeling of viscoplastic deformation of metals is very well developed; i.e., based on the so-called internal variable formalism in thermodynamics of irreversible processes (Coleman and Gurtin, 1967; Lubliner, 1973; Lemaitre and Chaboche, 1990; Chaboche, 1989; Arnold and Saleeb, 1994; Arnold et al., 1994a, 1995; Freed and Walker, 1993; Chaboche, 2008; Horstemeyer and Barnmann, 2010; and Baig et al., 2023). A larger number of specialized forms of unified viscoplastic models (e.g., isotropic or anisotropic, fully associative or nonassociative, etc.) have been successfully applied in recent years to different high-temperature metals, alloys, and composite material systems (Lemaitre and Chaboche, 1990; Arnold et al., 1994a, 1995; Freed and Walker, 1993; Krausz and Krausz, 1996; Krempl, 1996, Hart, 1976;

Hui, 1985; Kumar et al., 1980; Robinson, 1987; and Saleeb and Wilt, 1993). In the present paper, a fully associative generalized viscoelastoplastic potential framework[1] (Arnold and Saleeb, 1994; Arnold et al., 1994a,b, 1995, 2001; Saleeb and Wilt, 1993; Saleeb et al., 2001; Saleeb and Arnold, 2001, 2004) is utilized to represent a rather comprehensive set of experimental results performed on the titanium alloy TIMETAL 21S[2] (Lissenden et al., 2007). TIMETAL 21S is a β-titanium alloy with a nominal composition of Ti-15Mo-3Nb-3Al-0.2Si (% weight). Depending on the stress/deformation levels, this material was found to exhibit both reversible and irreversible behavior with marked rate dependency in each regime at elevated temperature.

The objective of the present paper is the assessment of the predictive ability of a coupled multimechanism viscoelastoplastic model, known as GVIPS (see Saleeb et al., 2001, Saleeb and Arnold, 2004) with a specific form for the material hardening function that has a true saturation value (or limit state) associated with it, in the context of cyclic deformation behavior. To that end the numerous cyclic experiments both uninterrupted and interrupted with 2-hr relaxation periods around the hysteresis loop generated by Lissenden et al., 2007 will be predicted. The uninterrupted cyclic tests indicate the loading rate dependence (when conducted in strain-control) and ratcheting behavior (when conducted in stress-control or strain-control with stress limits) of the material. The stress rate was equivalent to the elastic strain rate. The two interrupted tests contain 12 2-hr strain hold periods, one or more happening in each quadrant of the stress-strain space, wherein stress relaxation occurs. These relaxation response histories, particularly due to the prior load history, then provide excellent information for verifying the accuracy and/or guiding the development of constitutive models at high temperature.

In the current GVIPS model the viscoelastic part utilizes the concept of an equilibrium stress, leading to rate dependency upon instantaneous loading, as well as to a unique limiting state of elastic deformation at infinite times (Saleeb and Arnold, 2001 and Arnold et al., 2001). The viscoplasticity formulation accounts for both nonlinear kinematic hardening and static-recovery mechanisms (see Saleeb et al., 2001, Saleeb and Arnold, 2004). The implicit numerical-integration aspects, as well as the computational aspects concerning the automation of material-parameter-estimation procedures using the software called *COMPARE* (COnstitutive Material PARameter Estimator) has been reported in Saleeb et al., 2002 and 2003. We refer the reader to the above paper (and other references therein) for further details.

This paper begins with a brief outline of the general fully associative framework for several interacting mechanisms of the viscoelastic and viscoplastic types, leading to the governing flow and evolutionary rate equations. In the next section, the general characterization strategy is discussed with the specific values for the various material parameters, given a six-mechanism viscoelastic (reversible) and three-mechanism viscoplastic (irreversible) representation of the model. This is then followed by sections that describe in detail the results of the comparison of both the characterization tests (see Saleeb et al., 2001) and the validation tests selected within Lissenden et al., 2007.

Generalized Viscoelastoplastic Potential Structure (GVIPS)

Here, the basic equations governing the behavior of a material element are summarized. The discussion is limited to the case of small deformations and isothermal conditions, in which the initial (virgin) state is assumed to be stress free (as well as all initial values of internal state parameters are assumed zero) throughout. Here, and for the remainder of the paper, a Cartesian reference frame is

[1] This framework falls into the category of phenomenological (or macroscopic) material representation based on continuum mechanics and internal state variables and has been labeled by Arnold and Saleeb as belonging to the (GVIPS) Generalized VIscoelastoplastic with Potential Structure) class of material models.

[2] TIMETAL 21S is a registered trademark of TIMET, Titanium Metals Corporation.

utilized, along with index notation (wherein summation is implied for repeated subscripts). However, for convenience, we also utilize superscript letters placed between parentheses as indices to identify sets of internal state parameters and when needed the summation over these will be indicated explicitly by the summation symbol.

All equations are written for the general 3D (three-dimensional) case; but the forms are directly applicable in subspaces (e.g., 2D plane-stress or plane-strain, etc.); see (Saleeb and Wilt, 1993; Saleeb et al.,1998, 1999). For conciseness, we define the total number of dissipative viscoelastic state variables (each of the second-order tensor type) as M; i.e., the corresponding nonequilibrium stress tensors (Saleeb and Arnold, 2001; and Arnold et al., 2001) are $q_{ij}^{(a)}(a=1,2,...,M)$ and their associated conjugate (strain-like) tensors are $p_{ij}^{(a)}$. In addition, we define the equilibrium stress tensor $(\sigma_s)_{ij}^{(a)}$ and its strain conjugate as ε_{ij}^{ve}. Similarly, for the viscoplastic mechanisms, we use the notation $\alpha_{ij}^{(b)}(b=1,2,...,N)$ for the back stresses (kinematic hardening) and $\gamma_{ij}^{(b)}$ for their conjugate or dual (strain-like) variables, for a total of N viscoplastic (second-order) tensorial state variables.

Potentials and State Equations

In accordance with the basic hypothesis of the additive decomposition of total strain tensor, ε_{ij}, into three components, that is a reversible (i.e., elastic/viscoelastic), ε_{ij}^{ve}; an irreversible (i.e., viscoplastic), ε_{ij}^{vp}; and a free thermal strain, ε_{ij}^{th} component; we have:

$$\varepsilon_{ij} = \varepsilon_{ij}^{ve} + \varepsilon_{ij}^{vp} + \varepsilon_{ij}^{th}, \tag{1}$$

Similarly, an additive decomposition for the two fundamental potentials, that is, the Gibbs, complementary function, Φ, and dissipation function, Ω, are assumed:

$$\Phi\left(\sigma_{ij},\alpha_{ij}^{(b)},q_{ij}^{(a)}\right) = \Phi_R\left(\sigma_{ij},q_{ij}^{(a)}\right) + \Phi_{IR}\left(\alpha_{ij}^{(b)}\right), \tag{2}$$

$$\Omega\left(\sigma_{ij},\alpha_{ij}^{(b)},q_{ij}^{(a)}\right) = \Omega_R\left(\sigma_{ij},q_{ij}^{(a)}\right) + \Omega_{IR}\left(\alpha_{ij}^{(b)}\right), \tag{3}$$

where the functional dependencies on the external (σ_{ij}) and internal $\left(q_{ij}^{(a)}\right)$ and $\left(\alpha_{ij}^{(b)}\right)$ state variables, with (a = 1,2,…,M) and (b = 1,2,…,N), and the conjugate variables ε_{ij}^{vp} (also ε_{ij}), ε_{ij}^{ve} (also $p_{ij}^{(a)}$), and $\gamma_{ij}^{(b)}$, respectively, are given by the following equations of state:

$$\varepsilon_{ij} - \varepsilon_{ij}^{vp} = \frac{\partial \Phi_R}{\partial (\sigma_s)_{ij}}, \tag{4}$$

$$\varepsilon_{ij}^{ve} = \frac{\partial \Phi_R}{\partial q_{ij}^{(a)}}, \tag{5}$$

$$\gamma_{ij}^{(b)} = \frac{\partial \Phi_{IR}}{\partial \alpha_{ij}^{(b)}} \tag{6}$$

The corresponding rate forms are then

$$\dot{\varepsilon}_{ij} - \dot{\varepsilon}^{vp}_{ij} = \frac{\mathrm{d}}{\mathrm{d}t}\frac{\partial \Phi_R}{\partial (\sigma_s)_{ij}} = \frac{\partial^2 \Phi_R}{\partial (\sigma_s)_{ij}\, \partial (\sigma_s)_{kl}} (\dot{\sigma}_s)_{kl}, \tag{7}$$

$$\dot{\varepsilon}^{ve}_{ij} = \frac{\mathrm{d}}{\mathrm{d}t}\frac{\partial \Phi_R}{\partial q^{(a)}_{ij}} = \frac{\partial^2 \Phi_R}{\partial q^{(a)}_{ij} \partial q^{(a)}_{kl}} \dot{q}^{(a)}_{kl}, \tag{8}$$

$$\dot{\gamma}^{(b)}_{ij} = \frac{\mathrm{d}}{\mathrm{d}t}\frac{\partial \Phi_{IR}}{\partial \alpha^{(b)}_{ij}} = \frac{\partial^2 \Phi_{IR}}{\partial \alpha^{(b)}_{ij} \partial \alpha^{(b)}_{kl}} \dot{\alpha}^{(b)}_{kl} \quad \text{or} \quad \dot{\alpha}^{(b)}_{kl} = \left[\frac{\partial^2 \Phi_{IR}}{\partial \alpha^{(b)}_{ij} \partial \alpha^{(b)}_{kl}} \right]^{-1} \dot{\gamma}^{(b)}_{ij}, \tag{9}$$

where the above equation is the internal constitutive rate equations for the internal (nonequilibrium) state variable for each hardening mechanism.

The corresponding flow and evolution (rate) equations are similarly obtained from the dissipation function and are as follows:

$$\dot{\varepsilon}^{vp}_{ij} = \frac{\partial \Omega_R}{\partial \sigma_{ij}}, \tag{10}$$

$$\dot{p}^{(a)}_{ij} = \frac{\partial \Omega_R}{\partial q^{(a)}_{ij}}, \quad a = 1, 2, \ldots M, \tag{11}$$

$$\dot{\gamma}^{(b)}_{ij} = -\frac{\partial \Omega_{IR}}{\partial \alpha^{(b)}_{ij}}, \quad b = 1, 2, \ldots N, \tag{12}$$

Note in Equation (5) only a single viscoelastic strain component is associated with all viscoelastic stress components. Also, for the viscoelastic response, the total stress is decomposed into an equilibrium stress, $(\sigma_s)_{ij}$, and a nonequilibrium (dissipative) reversible stress, q_{ij}; i.e.,

$$(\sigma_s)_{ij} = \sigma_{ij} - q_{ij}, \quad \text{where } q_{ij} = \sum_{a=1}^{M} q^{(a)}_{ij}, \tag{13}$$

and for the viscoplastic response, the total stress is decomposed again into an equilibrium, $(\sigma_{ij} - \alpha_{ij})$, and nonequilibrium, α_{ij} component; where

$$\alpha_{ij} = \sum_{b=1}^{N} \alpha^{(b)}_{ij}, \tag{14}$$

The above GVIPS framework attempts to capture the underlying physical processes associated with microscopic defects (e.g., dislocations, grain boundaries, voids etc. in metals) and their complicated interactions which span an entire spectrum of length scales (i.e., from the "atomistic (nano) to the microscale," to the "mesoscale" to the final "macroscale") by introducing the notion of multiplicity of mechanisms in the mathematical description. These mechanisms, reflecting the vastly different interactions, give rise to the introduction of an aggregate of individual internal state tensorial variables

(i.e., $q_{ij}^{(a)}$ and $\alpha_{ij}^{(b)}$) that account for interactions at different length scales, that is, "short" range between dislocations and other dislocations, and "long" range between a well-developed dislocation cell or subgrain and other defects and interfaces. In addition to the differences in "microstructural" length scales, the time rates of change governing their dynamics are also known to be vastly different, hence the notion of multiple (or spectrum of) characteristic relaxation times in the GVIPS formulation, i.e., $M_{ijkl}^{(a)}$ and $\eta_{ijkl}^{(a)}$ of Equations (15) and (17). The use of multimechanisms (embedding the effects of many time/length scales) in the GVIPS class of formulation enables the specialization of this general model into simpler (more restricted in scope) formulations, e.g., purely elastic, linear viscoelastic, classical rate-independent elastoplastic, as well as more elaborate forms of hereditary descriptions (involving viscous effects, nonlinear hardening, dynamic recovery, thermal/static recovery, relaxation, ratchetting or shakedown phenomena under load cycles) to name a few.

Specific Functional Forms

For concreteness, the specified functional forms that have been used in our previous work (Arnold et al., 1994a,b; 1995; Saleeb and Wilt, 1993; Saleeb and Arnold, 2001; Arnold et al., 2001; Saleeb et al, 2001; Saleeb and Arnold, 2004) and will be used for the most part herein are summarized below. These forms are quadratic for the viscoelastic contribution and essentially the same "power-type" nonlinear forms previously used for the viscoplasticity functions $\bar{H}_{(b)}$, Ω_1, and $\Omega_2^{(b)}$ in terms of the invariants of their respective arguments $\alpha_{ij}^{(b)}$, $\left(\sigma_{ij}-\alpha_{ij}\right)$ and $\alpha_{ij}^{(b)}$, see Equations (16), (18), and (20).

The specific forms for the reversible and irreversible potentials and driving functions are as follows:

$$\Phi_R = \Phi_R\left(\sigma_{ij}, q_{ij}^{(a)}\right) = \frac{1}{2}\left(\sigma_s\right)_{ij} E_{ijkl}^{-1}\left(\sigma_s\right)_{kl} + \frac{1}{2}\sum_{a=1}^{M} q_{ij}^{(a)}\left[M_{ijkl}^{(a)}\right]^{-1} q_{kl}^{(a)} + \sum_{a=1}^{M} q_{ij}^{(a)} p_{ij}^{(a)}\,, \tag{15}$$

$$\Phi_{IR} = \Phi_{IR}\left(\sigma_{ij}, \alpha_{ij}^{(b)}\right) = \sigma_{ij}\varepsilon_{ij}^{vp} + \sum_{b=1}^{N} \bar{H}_{(b)}\left(G^{(b)}\right), \tag{16}$$

and

$$\Omega_R = \frac{1}{2}\sum_{a=1}^{M} q_{ij}^{(a)}\left[\eta_{ijkl}^{(a)}\right]^{-1} q_{kl}^{(a)}\,, \tag{17}$$

$$\Omega_{IR} = \Omega_1\left(F\right) + \sum_{b=1}^{N} \Omega_2^{(b)}\left(G^{(b)}\right), \tag{18}$$

where

$$F = \frac{1}{2\kappa^2}\left(\sigma_{ij}-\alpha_{ij}\right)\Lambda_{ijkl}\left(\sigma_{ij}-\alpha_{ij}\right) - 1 \tag{19}$$

$$G^{(b)} = \frac{1}{2k_{(b)}^2}\left(\alpha_{ij}^{(b)}\Lambda_{ijkl}\alpha_{kl}^{(b)}\right) \tag{20}$$

and the specific functions

$$\Omega_1(F) = \int \frac{\kappa^2 F^n}{2\mu} dF,$$
$$\Omega_2^{(b)}\left(G^{(b)}\right) = k_{(b)}^2 \int \frac{r\left(G^{(b)}\right)}{h\left(G^{(b)}\right)} dG^{(b)}, \tag{21}$$
$$\bar{H}_{(b)} = k_{(b)}^2 \int \frac{1}{h\left(G^{(b)}\right)} dG^{(b)},$$

Note in the above, E_{ijkl} and $M_{ijkl}^{(a)}$ are fourth-order tensors of viscoelastic stiffness moduli (with E_{ijkl}^{-1} and $\left[M_{ijkl}^{(a)}\right]^{-1}$ being the corresponding compliance tensors); $\eta_{ijkl}^{(a)}$ (a = 1,2,...,M) are the fourth-order tensorial viscosity coefficients associated with the a^{th} dissipative viscoelastic mechanism; the Ω_1 and $\Omega_2^{(b)}$ are the inelastic dissipations due to plastic hardening and static (thermal) recovery, respectively; and each $\bar{H}_{(b)}$ is taken to be a nonlinear function of the corresponding viscoplastic internal state tensor $\alpha_{ij}^{(b)}$. To emphasize the functional dependency in the potentials, e.g., Φ_R, Φ_{IR}, and $\bar{H}_{(b)}$, the corresponding arguments are shown in parentheses.

The only remaining functions that need to be assumed are those defining the competitive processes within a material, that is the hardening and recovery terms. The function that drives the thermal recovery is taken as previously to be a "power-type" function, that is,

$$r\left(G^{(b)}\right) = R_{(b)}\left[G^{(b)}\right]^{m_{(b)}} \tag{22}$$

and the saturating form of the hardening function, $h(G^{(b)})$, which was introduced in Saleeb and Arnold, 2004 and explicitly possess a limit state in which hardening will cease, i.e., $h(G) = 0$, whenever the now explicit hardening threshold, $k_{(b)}$, is exceeded irrespective of the exponent, β, is utilized:

$$h_{sat}\left(G^{(b)}\right) = H_{(b)}\left(1 - \sqrt{G^{(b)}}\right)^{\beta_{(b)}} \tag{23}$$

This form can simulate saturation of a tensile curve (particularly difficult at lower temperatures where thermal recovery is naturally suppressed) while still accurately representing other loading histories, e.g., creep and relaxation, see Saleeb and Arnold, 2004.

Finally, in the above, κ, μ, n represent viscoplastic flow material constants, whereas the $\bar{H}_{(b)}$, $\beta_{(b)}$ are hardening material constants; $R_{(b)}$, $m_{(b)}$ are thermal recovery material constants; and constants $k_{(b)}$ are either "normalizing" or hardening threshold stresses, for the individual mechanism (b), where b = 1,2,…,N.

Resulting Multiaxial Flow and Evolution Equations

With the selection of the functional forms above, the present viscoelastoplastic model is now complete within the context of a fully associative potential structure. The following expressions constitute the governing associated flow and evolution equations, assuming multiaxial isotropic behavior.

$$\dot{\sigma}_{ij} = E_{ijkl}\left(\dot{\varepsilon}_{kl} - \dot{\varepsilon}^{vp}_{kl}\right) + \sum_{a=1}^{M} \dot{q}^{(a)}_{ij}\ , \tag{24}$$

$$\dot{q}^{(a)}_{ij} = M_{ijkl}\left(\dot{\varepsilon}_{kl} - \dot{\varepsilon}^{vp}_{kl}\right) - M_{ijkl}\eta^{-1}_{klrs}\dot{q}^{(a)}_{rs}\ , \tag{25}$$

$$\dot{\varepsilon}^{vp}_{ij} = \begin{cases} f(F)\gamma_{ij} & \text{if } \mathrm{F} \geq 0, \\ 0 & \text{otherwise,} \end{cases}, \tag{26}$$

$$\dot{\alpha}^{(b)}_{ij} = Q^{(b)}_{ijkl}\left[\dot{\varepsilon}^{vp}_{kl} - \frac{r\left(G^{(b)}\right)}{h\left(G^{(b)}\right)}\pi^{(b)}_{kl}\right],\ \text{if } \pi^{(b)}_{kl}\cdot(\sigma_{kl} - \alpha_{kl}) \geq 0 \tag{27}$$

where

$$\begin{gathered} Q^{(b)}_{ijkl} = \left[\frac{\partial^2 \bar{H}_{(b)}}{\partial\alpha^{(b)}_{ij}\partial\alpha^{(b)}_{kl}}\right]^{-1} = h\left(G^{(b)}\right)\left[Z_m + \frac{h'\left(G^{(b)}\right)}{h\left(G^{(b)}\right)\left[1 - \frac{h'\left(G^{(b)}\right)}{h\left(G^{(b)}\right)}\left\{2\kappa^2_{(b)}G^{(b)}\right\}\right]}\alpha^{(b)}_{ij}\alpha^{(b)}_{kl}\right], \\ \gamma_{ij} = \Lambda_{ijkl}(\sigma_{kl} - \alpha_{kl});\ \ \pi^{(b)}_{kl} = \left(\Lambda_{klij}\alpha^{(b)}_{ij}\right) \\ q_{ij} = \sum_{a=1}^{M} q^{(a)}_{ij},\quad \alpha_{ij} = \sum_{b=1}^{N}\alpha^{(b)}_{ij}, \end{gathered} \tag{28}$$

and

$$h'(\cdot) = \frac{1}{k^2_{(b)}}\frac{\partial h(\cdot)}{\partial G^{(b)}}, \tag{29}$$

Note Z_m is the "generalized" inverse of Λ_{ijkl} see Saleeb and Wilt, 1993 for further elaboration on this. Details regarding the numerical solution of these equations have been discussed previously, see Saleeb and Wilt, 1993; Saleeb et al., 2001. Furthermore, note that the flow and evolutionary loading conditions (Eqs. (26) and (27)) are slightly modified as compared to this previous work, due to our recent consideration of multiaxial ratchetting behavior as illustrated herein. Specifically, the inequality in Equation (27) is utilized to define the case of "loading" for the internal viscoplastic state $\alpha^{(b)}_{ij}$, whereas for unloading $\pi^{(b)}_{kl}\cdot(\sigma_{kl} - \alpha_{kl}) < 0$ the $Q^{(b)}_{ijkl}$ operator is taken as a constant matrix wherein a very small value of $G^{(b)}_0$ is utilized (assumed here to be 0.001).

Model Characterization

Outline of the General Strategy

The most important, and often most difficult, aspect of modeling the behavior of a given material at elevated temperature is obtaining the required material functions, e.g., $f(F)$ and $g(G)$, for viscoplasticity and associated material parameters. The difficulty associated with this process typically stems from not only the variety in mathematical forms for the material functions (e.g., power law, exponential,

hyperbolic sine, etc.), but also the fact that given the material functions there is no unique set of material parameters for any given load path. Therefore, numerous iterations and difficult compromises are required before a final set of material parameters (for the assumed material functions) can be obtained.

Traditionally, characterization has been accomplished through basic trial and error procedures (i.e., graphical and/or mechanistic) which attempt to fit the predicted response from the constitutive model to that response exhibited by the experimental test data. These approaches, however, are rather limited, difficult, and many times less than fruitful for more general and sophisticated constitutive models. This is particularly true when dealing with models that possess a very large number[3] of material constants that; (i) are often lacking in their direct physical interpretation (not the case in the present model), (ii) may have vastly different magnitudes, and (iii) are highly interactive with each other. Further complications also arise when many experimental tests of various types (i.e., stress-, strain-, or mixed-control) under transient and/or steady-state conditions, are expected to be simulated.

To overcome these difficulties, *COMPARE* was developed to enable a design engineer to easily and efficiently bridge this gap between constitutive theory and experimental test data, in which optimum material parameters are determined by minimizing the errors between experimental data and the correlated responses (Saleeb et al., 2001 and 2002). Within *COMPARE* the estimation of material parameters is cast as a minimum-error, weighted least-squares, multi-objective optimization problem; wherein, this optimization problem is solved using the Sequential Quadratic Programing Technique. *COMPARE* is sufficiently general to handle a comprehensive set of test data, under arbitrary load-control variables, multiaxial stress/strain state, and transient as well as steady-state response measurements.

Characterization of Material Parameters

Here, the primary objective in this paper is to characterize the corresponding material parameters for the current multimechanism, viscoelastoplastic model of the GVIPS class with kinematic hardening; given TIMETAL 21S an advanced titanium-based matrix commonly used in titanium matrix composites (TMC's). Previous work (Arnold et. al., 1994a,b, 1997, 2000; Saleeb et al., 2001 and Saleeb and Arnold, 2004) indicated that six viscoelastic mechanisms (i.e., M=6) were sufficient to adequately span the entire reversible load spectrum with the proper rate sensitivity at 650 °C and that a single viscoplastic transient mechanism (i.e., N=1) appeared insufficient to accurately (quantitatively) represent the irreversible domain over a wide stress range. In Saleeb and Arnold, 2004 it was shown that three viscoplastic submechanisms where sufficient to accurately simulate the irreversible deformation behavior of TIMETAL 21S at 650 °C. Therefore herein, the number of viscoelastic mechanisms is held fixed at six, with the 14 reversible material constants being those determined previously (see Arnold et al., 2001) and given in Table 1. Note a key assumption is that Poisson's ratios is identical in all three matrices E_{ijkl}, M_{ijkl}, and $\eta^{(a)}_{ijkl}$; thus making the fourth-order tensor moduli coaxial and given the assumption of material isotropy, these moduli take on the following form: $E_{ijkl} = E_s N_{ijkl}$, $M^{(a)}_{ijkl} = M_{(a)} N_{ijkl}$, and $\eta^{(a)}_{ijkl} = \rho_a M^{(a)}_{ijkl}$ where

$$N_{ijkl} = \left\{ \frac{\nu}{(1+\nu)(1-2\nu)} \delta_{ij}\delta_{kl} + \frac{1}{(1+\nu)} \left(\delta_{ik}\delta_{jl} + \delta_{il}\delta_{jk} \right) \right\},$$

With respect to the irreversible domain, 3+5M constants are required in total; where three (i.e., κ, μ, and n) are associated with the flow law which is driven by the equilibrium (effective) stress, and the

[3] In the specific model presented, the total number of material parameters required is $5 + 5N + 2M$ where N defines the number of viscoplastic mechanisms and M the number of viscoelastic.

remaining 5 per submechanism (three with the nonlinear hardening operator; i.e., H_b, β_b, and k_b, the hardening threshold, and two with the thermal recovery term; i.e., R_b and m_b are associated with the evolution of the nonequilibrium (back or internal stress). Here M will be fixed at 3.

All tests addressed are uniaxial, isothermal, experiments conducted at 650 °C, thus implying that the multiaxial material constants are typically generalized from their uniaxial counterparts. This need for generalization is precisely why a consistent multiaxial theory, such as that developed from a potential formulation, is imperative. The available data are quite extensive. The 11 tests (i.e., three tensile at different total strain rates, three relaxation, four conventional creep, one fully reversed cyclic test) used for characterizing the 3+5M viscoplastic material constants (M=3) are summarized in Table 2, while the remaining 9 tests (indicated by 87-X, described in detail in Lissenden et al., 2007) used to verify the predictive ability of the current GVIPS model are given in Table 3. Clearly, the GVIPS model can provide nonisothermal response by characterizing the model parameters at various temperatures of interest, see Arnold and Lerch, 2024, and Arnold et al.,2001.

TABLE 1.—VISCOELASTIC MATERIAL CONSTANTS FOR TIMETAL 21S AT 650 °C

Constants	Value					
E_s, GPa	21.733					
ν	0.365					
Mechanisms	a=1	a=2	a=3	a=4	a=5	a=6
$M_{(a)}$, GPa	41.37	6.895	21.120	6.523	3.965	3.434
$\rho_{(a)}$, s	0.5	50.0	974.0	9693.0	14460.0	28218.0

TABLE 2.—EXPERIMENTS USED FOR CHARACTERIZATION OF TIMETAL 21S AT 650 °C

Specimen ID	Test	Load rate	Limits	Mode	Additional
1	Tension	8.33×10^{-4}/s			
2	Tension	8.33×10^{-5}/s			
3	Tension	8.33×10^{-6}/s			
4	Creep	0.7 MPa/s			14 MPa
5	Creep	70 MPa/s			74 MPa
6	Creep	70 MPa/s			111 MPa
7	Creep	70 MPa/s			130 MPa
8	Relaxation	5.0×10^{-4}/s			0.0014
9	Relaxation	5.0×10^{-4}/s			0.004
10	Relaxation	5.0×10^{-4}/s			0.006
11	Cyclic	8.33×10^{-5}/s	±0.01	1	1¼ cycles

TABLE 3.—GVIPS VALIDATION EXPERIMENTS FOR TIMETAL 21S AT 650 °C, SEE LISSENDEN ET AL. (2007)

Specimen ID	Test	Mode	Load rate	Limits	R	Additional
87-04	Cyclic	1	0.001	±0.005	–1	1187 cycles
87-15	Cyclic	2	78 MPa/s	±276 MPa	–1	3661 cycles
87-16	Cyclic	2	0.39 MPa/s	+87/–44 MPa	–0.5	191 cycles
87-25	Cyclic	2	78 MPa/s	+280/–140 MPa	–0.5	104 cycles
87-41	Cyclic	1	0.00001	±0.005	–1	155 cycles
87-44	Cyclic	2	0.39 MPa/s	±87 MPa	–1	150 cycles
87-49	Cyclic	2	0.39 MPa/s	+88/–44 MPa	–0.5	201 cycles
87-21	Interrupted	1	0.001	±0.005	NA	
87-50	Interrupted	1	0.001	±0.005	NA	

It is important to realize from the outset, that the resulting set of material parameters is nonunique (due to the nonlinear nature of the problem), however if enough "data content"[4] is provided to *COMPARE* then it is believed that the final obtained parameters should be relatively independent of the initial guess and bounds provided. It is beyond the scope and intent of this paper, however, to define what constitutes this sufficient data content. For the purpose of the present exercise, the actual characterization process for the multimechanism viscoplastic portion of the model was divided into three stages given the fact that the viscoelastic constants were known from previous work, see Arnold et al., 2000 and 2001, that is: 1) determine the flow and hardening parameters (μ, n, H_b, β_b, and k_b) using the three tensile curves at different total strain rates, 2) determine the thermal recovery parameters (R_b and m_b) given the three relaxation, four conventional creep, and one multi-step creep tests while keeping the flow and hardening parameter estimates from step 1 fixed and 3) fit all 11 tests at one time to obtain final parameter estimates - this is accomplished by allowing all viscoplastic parameters to be active (using the material parameters found in steps 1 and 2 as initial starting values) but with tight upper and lower bounds around each parameter. *COMPARE* was utilized exclusively in all stages of the characterization process, with the resulting set of viscoplastic parameters being given in Table 4.

In the case of multiple viscoplastic mechanisms, it is important to remember that the bounds are selected so as to keep each mechanism separate from the other (as each mechanism should possess a unique internal clock, or effective time domain). Note that the initial starting value and both upper and lower bounds on the viscoplastic parameters were selected based on experience and physical meaning. For example, the maximum internal stress achievable (the hardening threshold, k_b), which will strongly influence when a tensile stress-strain response saturates, is equal to $\sum_{b=1}^{N} k_b$; where N is the total number of viscoplastic mechanisms. This value $\left(\sum_{b=1}^{N} k_b = (\sigma_{sat} - \sqrt{3}\kappa) / \sqrt{3}\right)$ can be estimated directly from the available constant strain-rate tensile (stress-strain curves) tests, provided they have saturated. For

[4] Data content is meant to imply the variety of experimental data provided not just quantity. In other words, if one only provided tensile data to *COMPARE* one should not expect the model to be able to accurately predict both creep and relaxation response (since the time duration of these types of tests far exceeds that of a tensile test). Similarly, if one provided only creep or relaxation data to *COMPARE*, one should not expect the model to accurately represent the typically shorter time domain tensile behavior of the material.

TABLE 4.—VISCOPLASTIC MATERIAL
CONSTANTS FOR TIMETAL 21S AT 650 °C

Constants	Characterized value		
κ, MPa	4.25		
n	1.016		
μ, GPa	2,212.64		
Mechanisms	b=1	b=2	b=3
k_b, MPa	57.0	56.9	43.5
H_b, GPa	19,000	3.11	1.42
β_b	1.0	6.65	4.5
R_b, 1/s	0.1511	1.54×10^{7}	0.017506
m_b	1.0	4.025	7.214

TIMETAL 21S it appears that this total amount is in the range of 91 to 223 MPa for the different strain rates used in the experiments. Note, in the above definition, σ_{sat} is defined to be the measured maximum stress, at the fully developed plastic/saturation state. Consequently, for the case of two and three mechanisms, the initial starting values for k_b are taken to be equal, i.e., $\kappa_{single}/3$ and then allowed to move from there. The lower bound for $\sqrt{3}\sum_{b=1}^{N} k_b$ being equal to the highest creep stress examined. Also, the threshold parameter κ represents the value of stress below which only reversible (albeit time-dependent or time-independent) behavior is present, i.e., no measurable inelastic behavior occurs. Thus, κ delineates the reversible and irreversible regimes. This is the reason why below κ only viscoelastic behavior need be considered; alternatively, when the stress state exceeds κ both viscoelastic and viscoplastic behavior are fully active. Finally, it is highly recommended that the values of the exponents (i.e., n, β_b, and m_b) be always taken greater than one to ensure proper behavior of the various derivatives. Values less than one can at times produce excellent correlations while at the same time provide peculiar response histories for other loading configurations.

Results

Comparison of GVIPS Response to Experimental Characterization Tests

In the following results, six viscoelastic mechanisms are included along with three viscoplastic mechanisms. In Figure 1 to Figure 4 the viscoelastoplastic correlations for, i) the tensile response of TIMETAL 21S over three orders of magnitude in total strain rate (i.e., $\dot{\varepsilon}=8.33\times10^{-4}$, 8.33×10^{-5}, and 8.33×10^{-6} sec^{-1}), ii) relaxation responses given three initial strain levels (i.e., e = 139, 400, and 602 με loading, respectively, to the following "peak" stress levels, σ =100, 240, and 343 MPa, all produced given a total loading strain rate of $\dot{\varepsilon}=8.33\times10^{-4}$ sec^{-1}, and iii) short term creep at three stress levels (i.e., σ = 72, 110, and 128 MPa) are shown, respectively. In the graphs, the solid lines denote experimental data and the dashed lines the model correlations. In the authors' opinions, these correlations are qualitatively very good given the very wide variety of loading conditions examined. Overall, the maximum quantitative correlation errors are between 1 to 12 percent for tension, cyclic and relaxation stress correlations and 20 to 40 percent in accumulated creep strain for the load history imposed in each test. This is well within typical experimental scatter, particularly when dealing with creep measurements which can show upwards of 200 to 300 percent variation.

The tensile response of TIMETAL 21S over three orders of magnitude in total strain rate (i.e., $\dot{\varepsilon} = 8.33\times10^{-4}$, 8.33×10^{-5}, 8.33×10^{-6} sec^{-1}) as well as its fully reversed cyclic response is shown in Figure 1 and Figure 2. Note herein the saturating hardening form introduced in Saleeb and Arnold, 2004) is utilized throughout. Figure 1 illustrates the experimental stress strain response histories (indicated by solid lines) and the corresponding correlated response via the saturated form (dashed lines). The correlation is very good over the entire range of loading rates and note the ability of the model to capture the saturation of the stress beyond 1 percent total strain. Note how only the 8.33×10^{-5} sec^{-1} strain rate test is quantitatively accurate with the lower and higher strain rates being quantitatively in greater error. This is expected, since the irreversible dissipative mechanisms (although stress dependent) must compromise over the entire time spectrum of all the experiments being correlated. Overall, the model appears to be able to accurately capture (both qualitatively and quantitatively) the actual strain rate dependency of the material. Similarly, in the case of cyclic loading (see Figure 2) the current saturating hardening form does a very good job of representing the real material behavior over the entire strain range. Although, it obviously does a poorer job matching the stress-strain behavior in quadrants three and four of the stress-strain space. Again, one sees as expected a compromise being made by COMPARE when fitting this response.

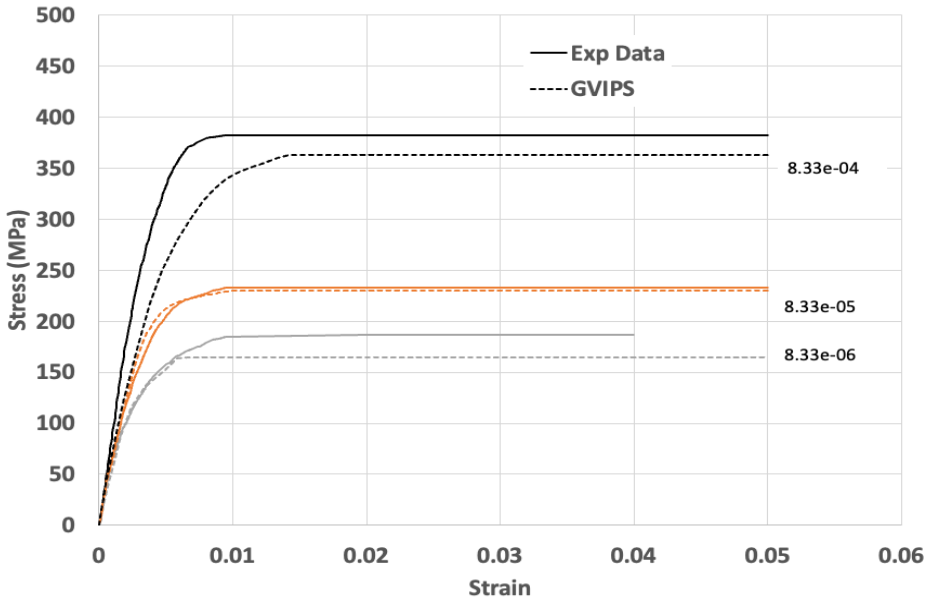

Figure 1.—Comparison of experiment (solid line) and correlated GVIPS (dashed line) stress-strain behavior of tension tests for three different total strain rates (8.33×10^{-4}, 8.33×10^{-5}, 8.33×10^{-5} 1/sec).

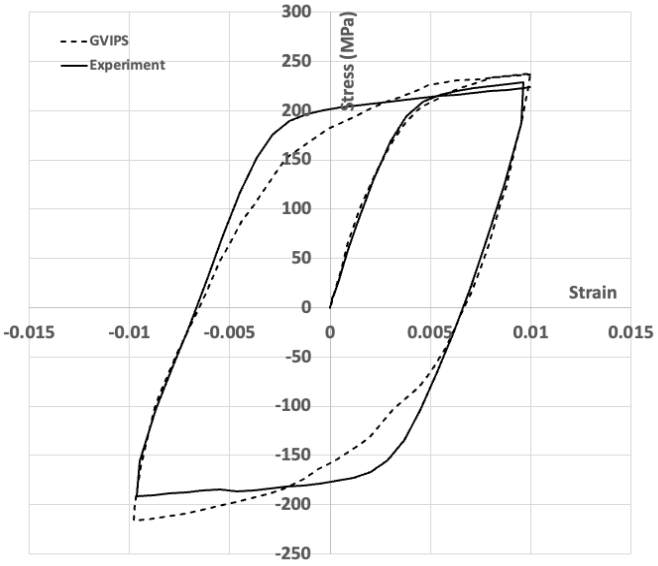

Figure 2.—Comparison of experiment and correlated stress strain behavior for fully reversed cyclic test at 8.33×10^{-5} sec^{-1} rate of loading.

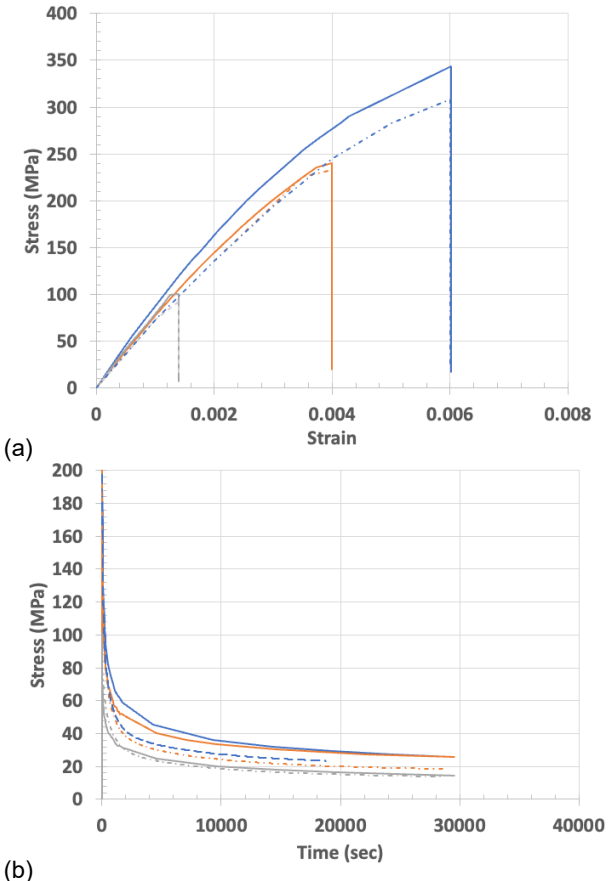

Figure 3.—Prediction of relaxation response (tests 8-10 in Table 2) showing (a) stress-strain and (b) stress-time response. Note solid lines are experimental response and dashed lines are GVIPS correlations assuming 3 viscoplastic mechanisms.

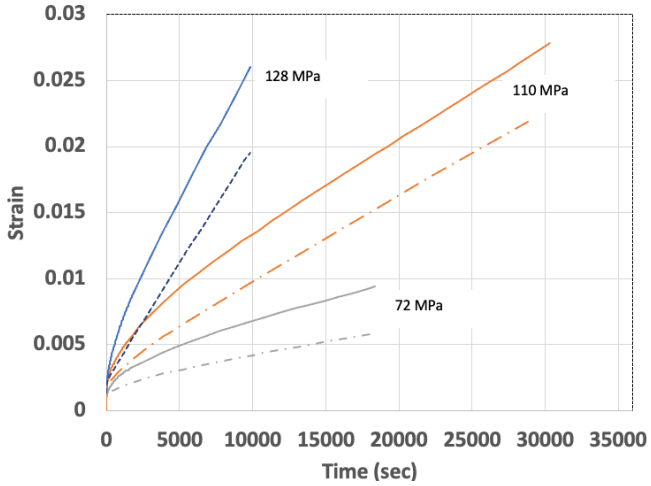

Figure 4.—Creep response of TIMETAL 21S at 72, 110, and 128 MPa. Solid lines are experimental results, and dashed lines are GVIPS correlations assuming 3 viscoplastic mechanisms.

Qualitatively the relaxation behavior exhibited by the material, shown in Figure 3, is very well captured by the model. This is particularly true regarding the primary relaxation feature, that is, the initially high stress reduction rate and overall large stress-drops at all stress levels. Note that the three starting relaxation stress levels in Figure 3 represent stress levels[5] that are: i) below the apparent yield, ii) within the knee (e.g., 115 to 330 MPa), and iii) near the ultimate stress level of the material (approximately 345 MPa). Also, the specimen-to-specimen repeatability is off by approximately 4 to 16 percent based on stress induced at a given strain level, with error increasing as the strain increases. Note GVIPS must repeatably produce the same response curve (for a given rate, 5.0×10^{-4} sec^{-1}) irrespective of the target relaxation strain. Also, Figure 3(b) shows the stress vs. time response for both experiment and GVIPS correlation, wherein here the vertical stress limit was capped at 200 MPa to enable better visualization of the stress history response. Therefore, given the repeatability error in the experiments the authors believe the model does a very good job of capturing the relaxation response accurately.

Similarly, when examining the creep response correlations given in Figure 4, the model again can capture qualitatively the stress dependence over the entire stress range, with the secondary creep rate as a function of stress being better correlated than the primary creep response. Note the initial (primary) creep rates are significantly underpredicted by the GVIPS model thus leading to the significant underprediction of the overall creep response regardless of the applied stress while the secondary (i.e., steady state) rate are almost identical. Further, because of the constant load-controlled creep test, the experimental results have both additional geometric effects and possibly creep damage (thereby leading to tertiary creep) included in them. Neither of these factors have been included in the numerical simulation/correlation. The influence of these factors is particularly evident during higher creep loading, where the inelastic strain rate during the experiment is significantly greater than that simulated (cf. σ =128 MPa in Figure 4).

[5] Given a 5.0×10^{-4} sec^{-1} total strain rate ramp-up history, see Figure 2.

It is important to note that if one were to focus on only one type of loading condition, superior correlations could of course be achieved for that class of loading. However, predictions of other classes of loading may severely suffer. For example, during a separate characterization process involving only the three tensile tests, excellent correlation was obtained, but at the expense of poor creep and relaxation behavior for a given set of material parameters. Conversely, when the model was calibrated for creep responses, poorer tensile and relaxation behavior were similarly predicted. Thus, when judging the "goodness" of a given model one must keep in mind the appropriate required "data content" for accurately capturing the full range of material behavior of interest. This ties into the concept of idealization consistency (see Arnold and Lerch, 2024) wherein one must consider theoretical, mechanistic, and numerical aspects of any given problem and ensure that no inconsistencies are present between these three categories. Also, it is important to include the proper meta data (e.g., associated with the characterization process) when capturing or documenting the constitutive model and its associated parameters for a given material. This requirement is extremely important, as will become self-evident in the next section, to ensure that a given model is not improperly utilized.

Predictive Capability of Multiple Mechanisms GVIPS Model

The predictive capability of GVIPS will be assessed using the complex cyclic loading experiments listed in Table 3 and executed and described by Lissenden et al., 2007 at a high homologous temperature (~0.4 T_m). These histories involved different loading modes such as strain control (mode 1), stress control (mode 2) and mixed (mode 3), in which strain control loading is applied with stress target values. Note the mode 3 tests, see Lissenden et al., 2007, will be addressed in a future paper due to differences in material batches described below. These tests are unique for testing the predictive capability of a constitutive model since they address the known effect of control mode on rate-dependent materials. Since in stress control the strain rate can increase significantly as inelastic deformation occurs whereas in strain control the rate is maintained irrespective of the amount of inelastic strain. Further, the uninterrupted stress controlled tests (87-16, 87-25, and 87-49) illustrate ratcheting (Hubel, 1966) due to the application of tensile mean stress and the interrupted tests (87-21 and 87-50 in Table 3) provide insight into the relaxation behavior in all four quadrants of the stress-strain space – thus enabling assessment of the chosen mathematical formulation of a given constitutive model such as GVIPS, see Arnold and Lerch, 2024. Remember the characterization of the current GVIPS was limited to response curves in the first quadrant only (i.e., tensile, creep, relaxation) and a single fully reversed cyclic response. Therefore, all experiments listed in Table 3 are legitimate validation experiments.

Figure 5 illustrates both the experimental and GIVPS simulation associated with specimen 87-04 and 87-41, the strain controlled cyclic response at 10^{-3} and 10^{-5} sec^{-1} rate, respectively. Overall, GVIPS does a reasonably good job of representing the cyclic behavior, although it is apparent that the model's response exhibits stiffer behavior than that of the experiments for both rates of loading. It is stiffer in the sense that the widths of the hysteresis loops are smaller than that of the experiments and the amount of hardening per cycle is less. This is particularly true for the slower, 10^{-5} sec^{-1}, rate case, 87-41 where even the tensile load-up is significantly higher than that of the experiment.

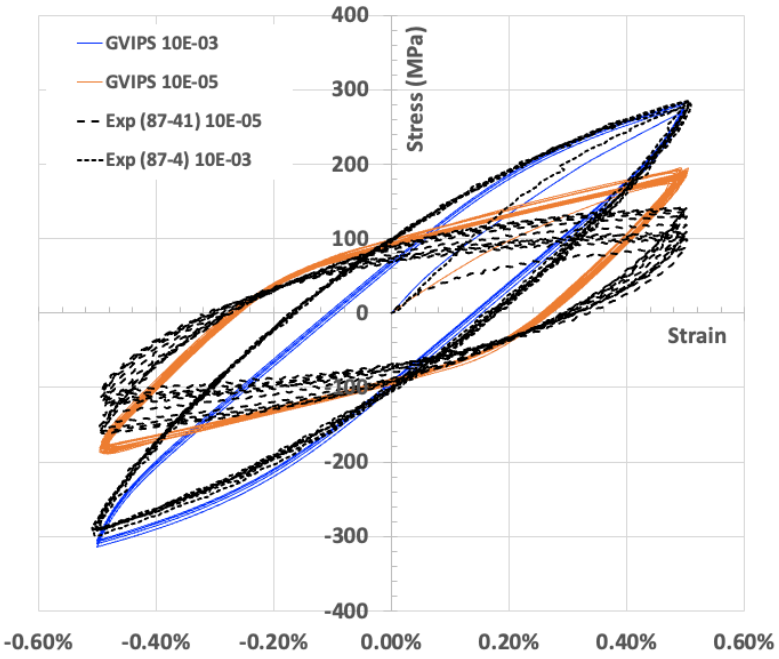

Figure 5.—Comparison of the experiment (colored) and GVIPS prediction (black) fully reversed cyclic stress-strain behavior at two strain rates.

The inability to capture the tensile load-up at the slower rate, when the model did a fine job of capturing the 8.33×10^{-6} rate case in Figure 1 prompted the plotting of the tensile loading phase of each of the experiments in Table 3, see Figure 6. Comparing these tensile loadings to those of the characterization data immediately revealed that the material tested by Lissenden et al., 2007, was significantly softer than that tested by Castelli, see Arnold et al., 1994a and Saleeb et al., 2001; particularly for the slower rate of loading associated with 10^{-5} sec^{-1}. The specimen-to-specimen repeatability for each rate is quite good however, except for the specimen 87-29 which shows significantly softer behavior than other tests at 10^{-3} sec^{-1} strain rate. Consequently, an investigation into the differences that might exist between the two batches of neat (fiber less) titanium matrix composite materials tested was undertaken with the results presented in Table 5. Clearly, only two distinct differences between the specimens are of note: 1) the shape of the actual test specimen –flat vs. round and 2) the number of plies through the specimen thickness. Neither of these two issues would seem to account for the significantly softer response of Lissenden's specimens. Note in Figure 6 a GVIPS simulation (brown dashed line) is included that corresponds to a total strain rate loading at 10^{-7} sec^{-1} which coincidently and serendipitously matches extremely well the initial load-ups associated with specimens 87-16, 41, 42, 44, 49 and 53. Comparing the cyclic behavior once again, see Figure 7, it is clear that a 10^{-7} sec^{-1} rate GVIPS simulation also matches the cyclic hardening behavior of the experiment 87-41 extremely accurately as well. Note in Figure 7 cycles 1-5, 10, 20, 30, 40 and 50 are shown for Exp 87-41 while cycles 1-37 are shown for the GVIPS simulation. As a result, the rate of loading for all the slower rate tests where double checked to ensure that they were indeed run at a rate of 10^{-5} sec^{-1}. This was indeed the correct rate.

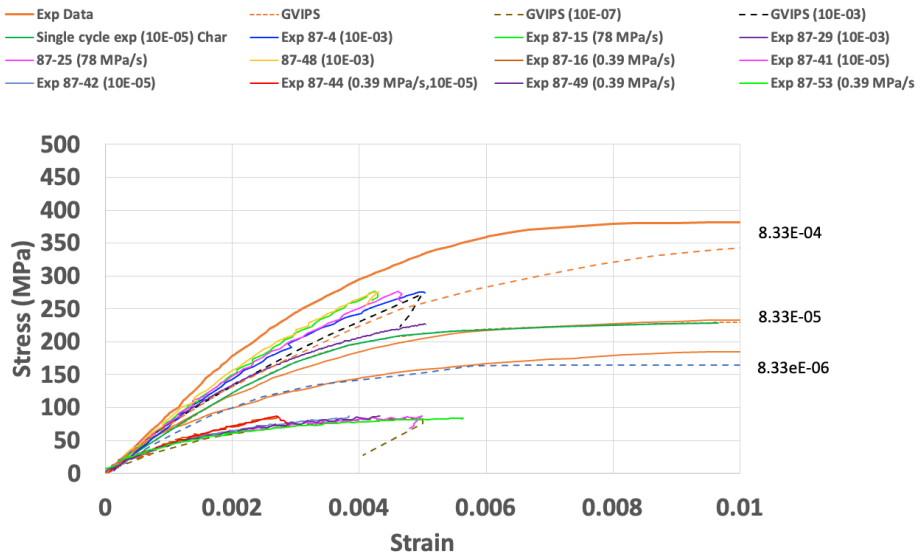

Figure 6.—Initial tensile loading for all tests in Table 4 plus the three tensile and cyclic tests in Table 2.

TABLE 5.—MATERIAL SPECIMEN INFORMATION TIMETAL 21S AT 650 °C

Specification	Castelli	Lissenden
Composition	Ti-15Mo-3Al-3Nb-0.2Si	Ti-15Mo-3Al-2.7Nb-0.2Si
Ply thickness	110 μm	110 μm
Number of plies	5	72
Total thickness	0.55 mm	8 mm
Grain size	ASTM 5	ASTM 5
	Equiaxed and homogeneous	Equiaxed and homogeneous
Specimen geometry	Rectangular dog bone	Round dog bone, 6.4 mm diam. gage
Heat treatment	8 hr at 621 °C in a vacuum	8 hr at 621°C in a vacuum

Figure 8 shows only 4 cycles, cycle 1, 50, 100 and 150 for both GVIPS (run at 10^{-7} sec^{-1} rate of loading) and the test 87-41 (run at 10^{-5} sec^{-1} rate of loading). Clearly GVIPS can capture the cyclic hardening very well. Figure 9 illustrates the maximum and minimum stress achieved per cycle for all 150 cycles during the test 87-41 and the GVIPS simulation. The GVIPS model under predicts the rapid early hardening associated with the experiment that saturates after approximately 80 cycles, as GVIPS reflects a more constant cyclic hardening that saturates after approximately 100 cycles. This difference in hardening is understandable since the model was characterized with only a single fully reversed cyclic load history and thus relies upon monotonic creep behavior to illuminate its cyclic hardening behavior.

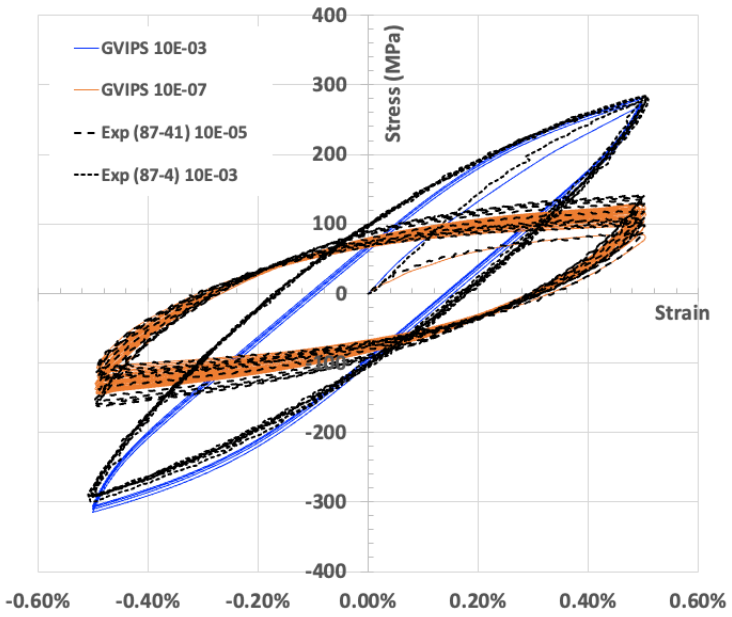

Figure 7.—Comparison of fully reversed, strain controlled (Mode 1) cyclic experimental data (at 10^{-3} and 10^{-5} sec^{-1}) and GVIPS simulations at 10^{-3} and 10^{-7} sec^{-1}.

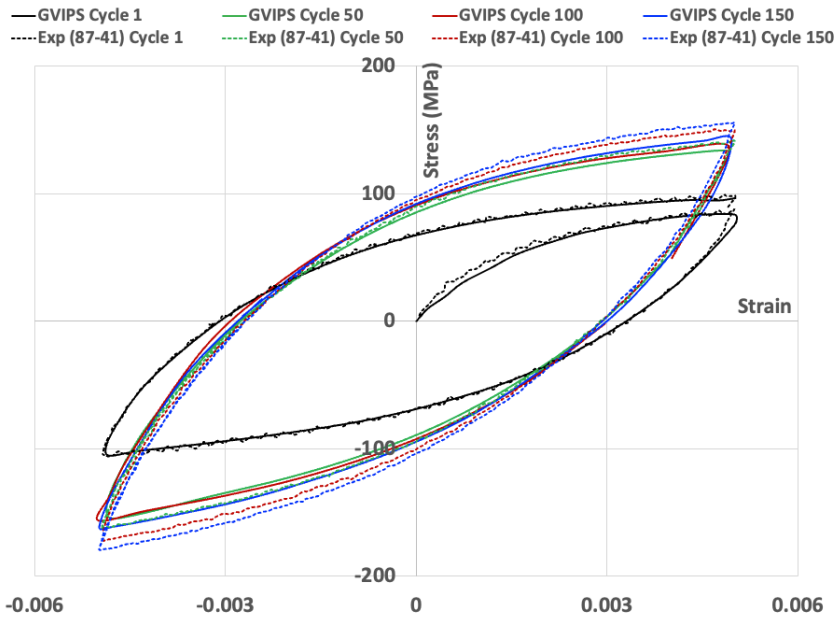

Figure 8.—Comparison of four fully reversed, strain controlled, cycles associated with experiment 87-41, cycle 1, 50, 100 and 150. Solid lines are simulations of GVIPS model run at 10^{-7} sec^{-1} rate while experiment was run at 10^{-5} sec^{-1}.

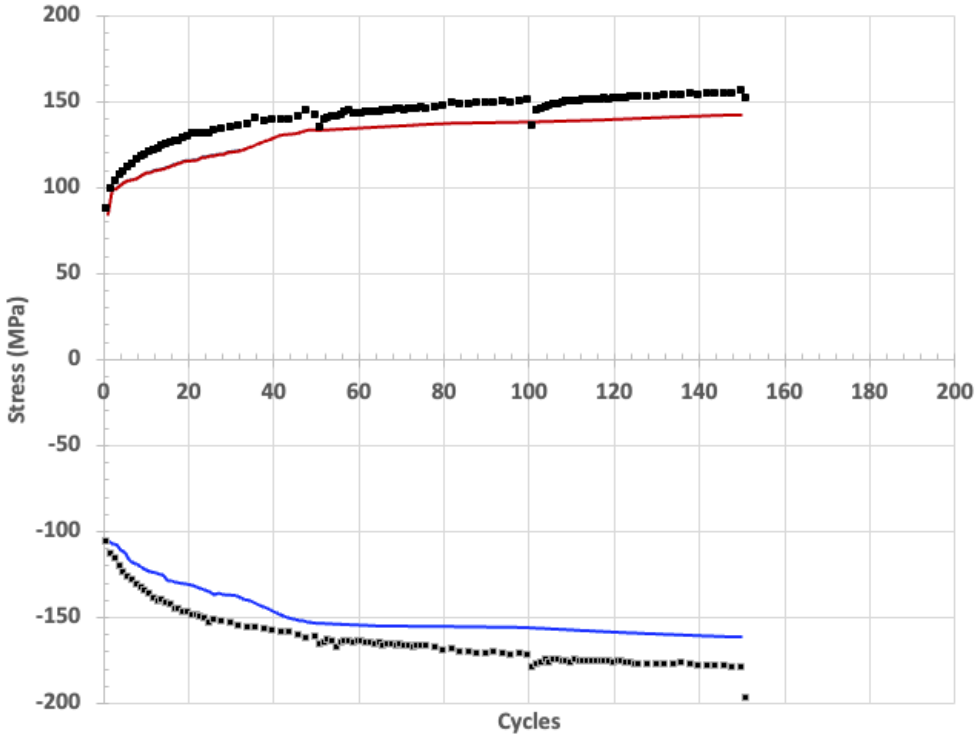

Figure 9.—Comparison of cyclic hardening rate, experiment (symbols) vs. GVIPS predictions (solid lines) for the strain controlled, 10^{-5} sec^{-1}, fully reversed cyclic test 87-41.

Figure 10 shows 4 cycles (cycle 1, 50, 100 and 150) for both GVIPS and test 87-44 run under stress control, at 0.39 MPa/sec rate which is elastically equivalent to a strain rate of 10^{-5} sec^{-1}. Clearly as expected one observes an increase in inelastic strain along the stress equal zero line, i.e., ratcheting of the strain as the number of cycles increase. As well as a decrease in the width of the hysteresis loop and a rotation of the hysteresis loop (which is consistent with hardening of the material). Here, since GVIPS was run at the actual experimental rate it should provide a significantly stiffer response for all cycles, as it does. Further, the GVIPS model exhibits the same qualitative character, i.e., increase in inelastic strain at zero stress (ratcheting) and rotation and decrease in hysteresis width, as the experimental results. Figure 11 shows the exact same results as Figure 10 except in this case the GVIPS model was run at the significantly slower, elastically equivalent, stress rate of 0.0039 MPa/sec and as expected based on previous tensile and cyclic results at this rate of loading the GVIPS model more accurately matches the inherently "softer" 72-ply specimen experimental results.

After the 155th cycle, in the case of mode 1 (experiment 87-41), a 12 hr relaxation test was performed at the hold strain of 0.005 m/m and initial stress of 164 MPa, whereas in the case of mode 2 (experiment 87-44), a 12 hr relaxation test was performed after the 150^{th} cycle and at a hold strain of 0.0027 m/m and initial stress of 117 MPa. The stress-time plots associated with both the experiment and GVIPS simulation (run at 10^{-5} sec^{-1}) are shown in Figure 12. Clearly, the stress relaxes asymptotically in both the experimental and simulation to a significantly lower stress value regardless of the previous number of cycles, initial stress or strain state. In the case of specimen 87-41 (mode 1) the final saturated stress is approximately 25 MPa while specimen 87-44 (mode 2) saturates at approximately 22.5 MPa. The GVIPS prediction of 87-41 starts at an initial stress of 140 MPa and ends at 20.45MPa while for the mode 2 case (stress controlled), 87-44, the initial stress is 87 MPa with saturation occurring at a value of 13.89 MPa. Note the shape of both the experimental and predicted response curves are very similar, while the difference between starting and ending points for the experimental response, is 47 and 2.5 MPa, and

GVIPS simulation, is 53 and 6.56 MPa, respectively. The difference between GVIPS and experimental values for both starting and end point are shown in Table 6 with the largest difference being associated with the stress-controlled test.

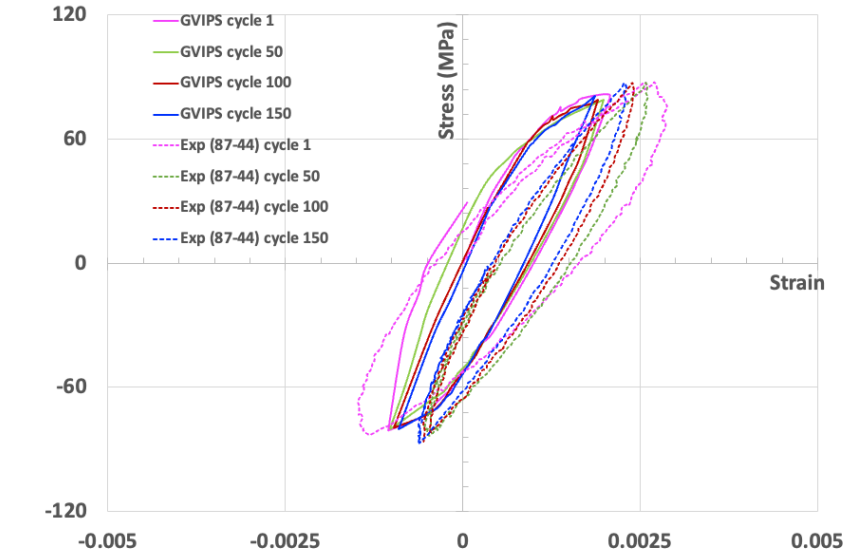

(a)

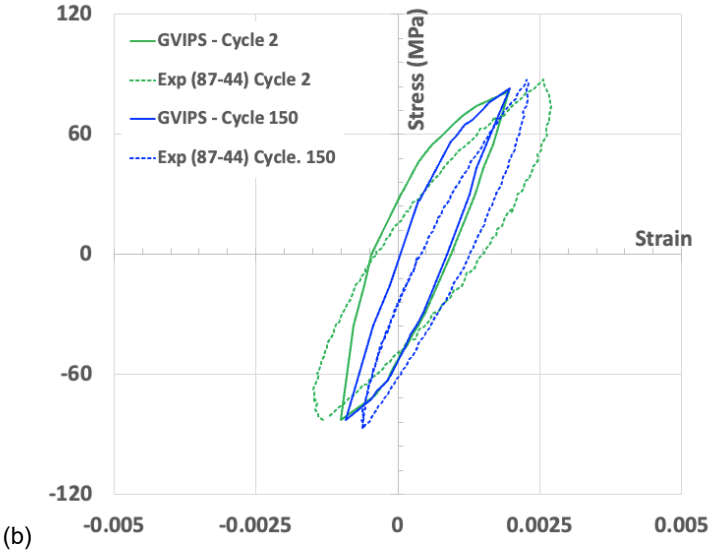

(b)

Figure 10.—Comparison of (a) four fully reversed, stress controlled (Mode 2), cycles associated with experiment 87-44, cycle 1, 50, 100 and 150 and (b) cycles 2 and 150. Solid lines are simulations of GVIPS model run at 0.39 MPa/sec rate for both experiment and GVIPS.

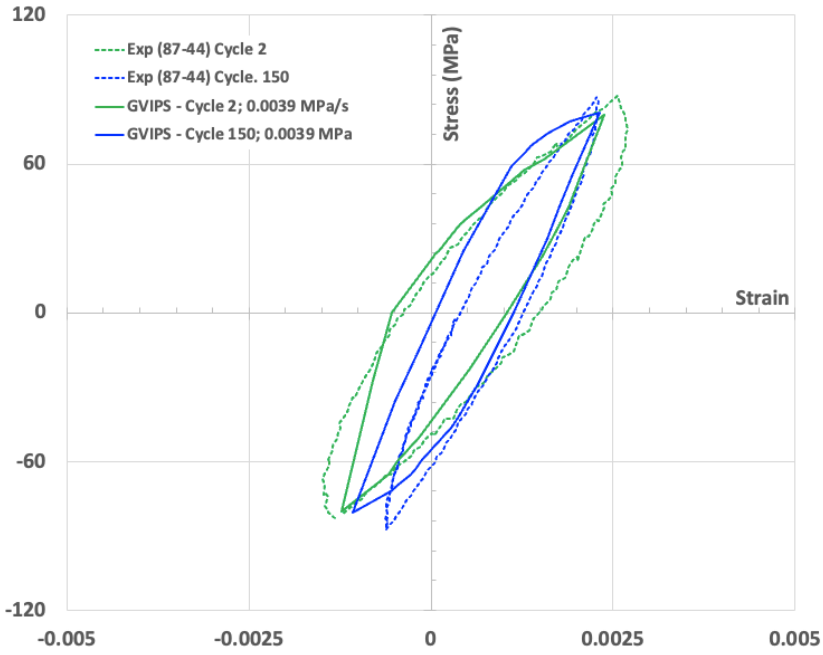

Figure 11.—Comparison of two fully reversed, stress controlled (Mode 2), cycles associated with experiment 87-44, cycle 2 and 150. Solid lines are simulations of GVIPS model run at 0.0039 MPa/sec rate for both experiment and GVIPS.

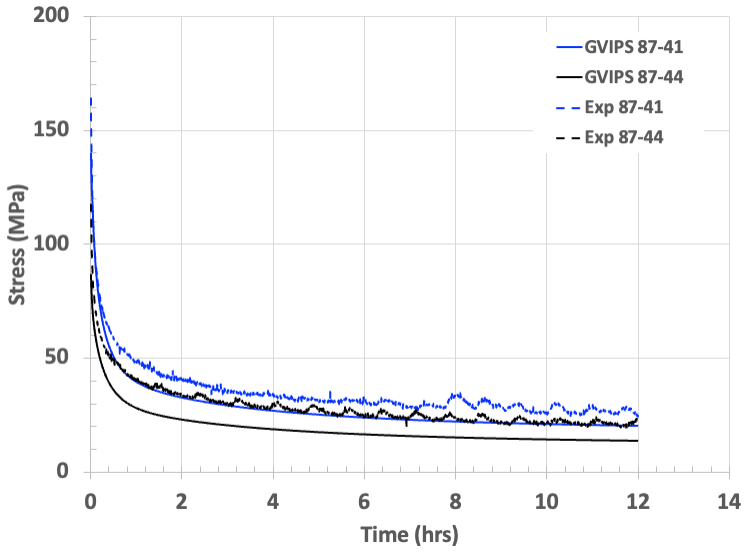

Figure 12.—Comparison of the stress relaxation response, stress vs. time, for the strain controlled (Exp 87-41) and stress controlled (Exp 87-44) experiments and associated GVIPS simulations after at least 150 cycles of deformation.

TABLE 6.—RELAXATION STARTING AND ENDING VALUES

Specimen	Starting value, MPa			Ending value, MPa		
	Exp	GVIPS	Error	Exp	GVIPS	Error
87-44	117	87	25%	22.5	13.88	38%
87-41	164	140	14.6%	25	20.45	18%

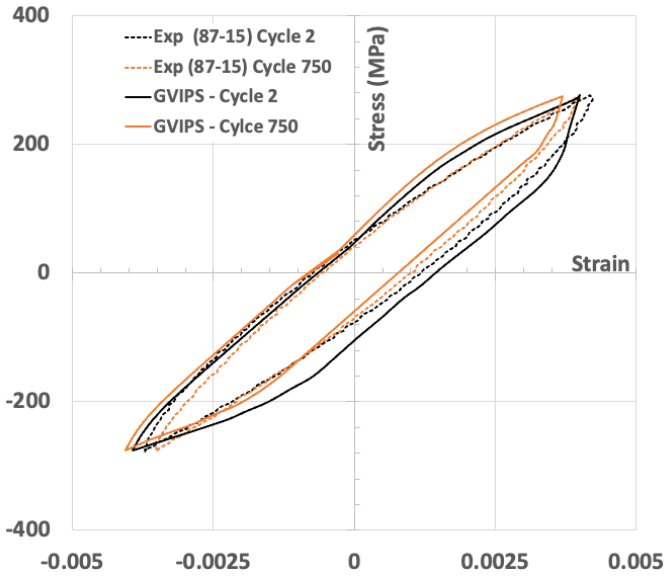

Figure 13.—Comparison of two fully reversed, stress controlled (Mode 2), cycles associated with experiment 87-15, cycle 2 and 750. Solid lines are simulations of GVIPS model run at 78 MPa/sec rate for both experiment and GVIPS.

Simulating the stress-controlled test 87-15 run at the higher stress rate of 78 MPa/s which is an elastically equivalent rate of 10^{-3} sec^{-1}, it is clear that the GVIPS model does a very good job of representing the response at both cycle 2 and cycle 750, see Figure 13. Once again, the GVIPS model exhibits more hardening than does the experiment, thus suggesting the need to provide some cyclic hardening information during characterization of the model parameters.

Next the influence of strain ratcheting will be examined by conducting a stress limited cyclic test, i.e., 87-25 see Table 3, assuming a higher rate of loading 78 MPa/sec with a tensile mean stress of 72 MPa such that the stress ratio $R = \sigma_{min}/\sigma_{max} = -0.5$ is applied. Figure 14 shows the cyclic response of both experiment (dashed lines) and GVIPS simulations (solid lines) for 5 selected cycles: 2, 5,10,15 and 30. Clearly, ratcheting is present with every cycle showing an increase in the mean strain accumulated along with slight hardening as evident by the decrease in width of each successive hysteresis loop, see Figure 15. Note GVIPS over predicts the initial ratcheting behavior, cycle 2 by approximately 65 percent while by the 30^{th} cycle it is only 5 percent over predicting. This is because the GVIPS model hardens at a more rapid rate initially than does the experiment. Figure 15 also shows that the accumulated ratchet (mean) strain after 30 cycles (or approximately 5.3 min of loading) exceeds 0.01 while it took approximately 5 hr to accumulate that much strain under monotonic creep at the equivalent mean stress of 72MPa, see Figure 4 and Figure 16. Finally, note TIMETAL 21S is a titanium alloy that was designed to be cyclically neutral and as exhibited by the various cyclic experiments performed by Lissenden (2007) although it slightly hardens it does indeed for the most part behave cyclically stable.

The actual accumulation of ratchet strain for a large number of cycles, like in the case of experiment 87-16, exhibits behavior like that of a creep response with an accelerating yet at decreasing rate zone (primary creep), constant zone (steady state creep) and then as damage begins to propagate another rapid acceleration zone (tertiary creep) appears, see Figure 16. Note that during test 87-16 a tensile mean stress of 22 MPa is present, thus one might expect the ratchet strain to increase at a pace equal to that of a creep test at this mean stress level (at least initially until some type of strength reduction damage begins to accumulate). However, as evident from Figure 16 the maximum, minimum and mean strain accumulation per cycle far exceed the strain accumulated due to a creep curve associated with 22 MPa (generated via GVIPS) and an experimental

curve associated with 72 MPa (see Figure 4). Therefore, demonstrating that ratchet strain accumulation under cyclic conditions is significantly more rapid than that produced by monotonic creep alone. Remember, previously it was demonstrated that the material associated with Lissenden et al., 2007 experiments is significantly "softer" than that used for characterization of the GVIPS model thus it is not surprising that the 72 MPa creep response is more in line with the mean strain accumulated in the 87-16 cyclic response. Further it is clear that the unified viscoelastoplastic GVIPS model (red line in Figure 16) can indeed capture the additional strain accumulation effect caused by cycling as compared to the monotonic 22 MPa GVIPS creep response. This is because during partial unloading into quadrant IV of the stress-strain space, the internal stress state is markedly reduced such that additional inelastic strain is accumulated with each cyclic reversal, as evidenced by the experimental results. Since the magnitude of accumulation is off from that observed in the experiment an additional curve associated with two orders of magnitude decrease in stress rate, 0.0039 MPa/s, is added to Figure 16 to demonstrate that the actual magnitude of accumulation most likely could be captured by the GVIPS model if it was recalibrated for Lissenden's "softer" 72 ply material. Note nonunified models would be unable to capture this effect often attributed to dynamic recovery (see Baig, et al., 2023, Lemaitre and Chaboche, 1990).

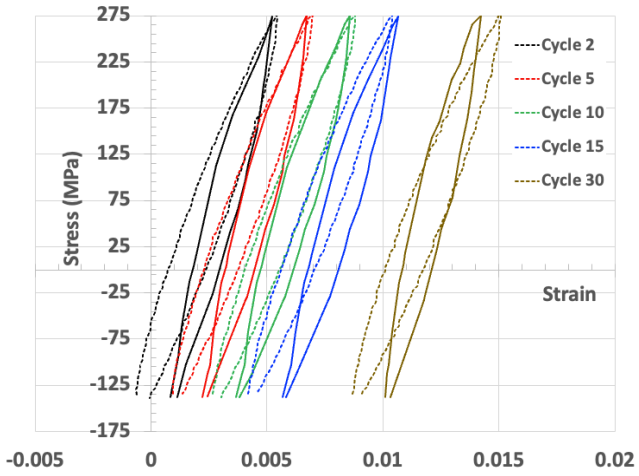

Figure 14.—Ratcheting hysteresis loops for stress controlled cyclic test (87-25) with an R= –0.5

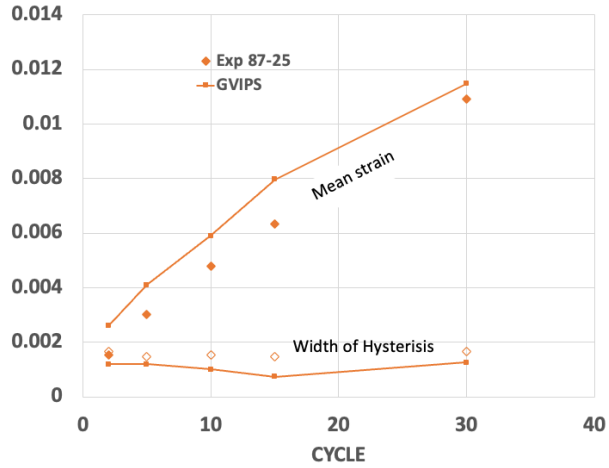

Figure 15.—Comparison of experiment 87-25 and GVIPS mean strain at zero stress and width of hysteresis loop.

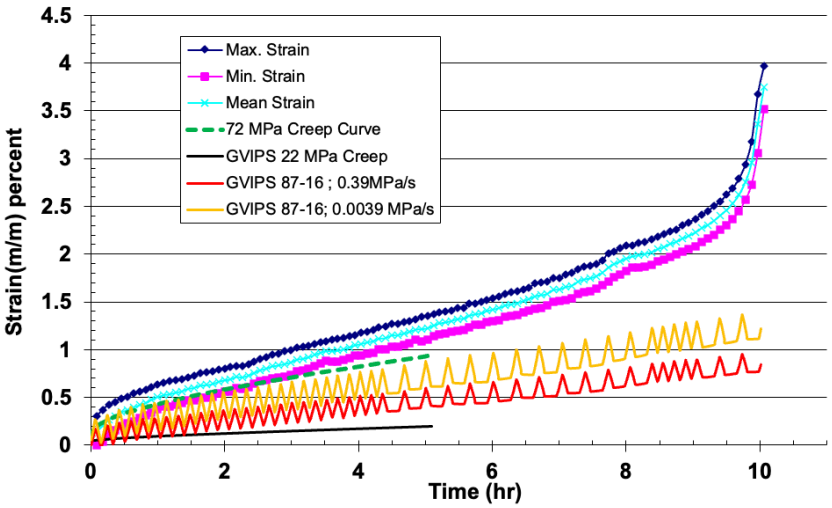

Figure 16.—Comparison of experiment 87-16 with GVIPS simulation. Note the flat lines in between the later GVIPS cycles are merely a plotting artifact and do not indicate hold times.

Interrupted Cyclic Response with Stress Relaxation Periods

Now relaxation behavior at various points along a hysteresis loop will be examined to understand if the functional forms chosen for the hardening ($h(G)$) and thermal recovery ($r(G)$) within the GVIPS model are sufficient to enable accurate prediction of complex cyclic material behavior at elevated temperature, 650 °C. Relaxation, the effect of holding the strain constant and allowing the stress to relax, in this case for 2 hr, is important as these relaxation histories, transcribed into the state-space (see Arnold and Lerch, 2024), provide critical information to define the functional forms associated with a given model. As stated in Lissenden et al., 2007, the specific location of each point shown in Figure 17 (around the hysteresis loop, i.e., A, B, C,…,P) was chosen to illuminate any difference or unusual time-dependent response in quadrants II and IV that does not occur in quadrants I and III. Note points D and J are of particular interest due to the lack of experimental results reported in the literature in this region. Similarly, points B or N, C or O and H and I are important as potential reversal of stress could occur here depending upon the magnitude of internal state and the applied loading. Lissenden's experimental results are unique in that different loading paths were also followed to quantify the path dependency of these responses if any. The interrupted cycles along with uninterrupted cycles were conducted on three separate specimens (87-50 and 87-21).

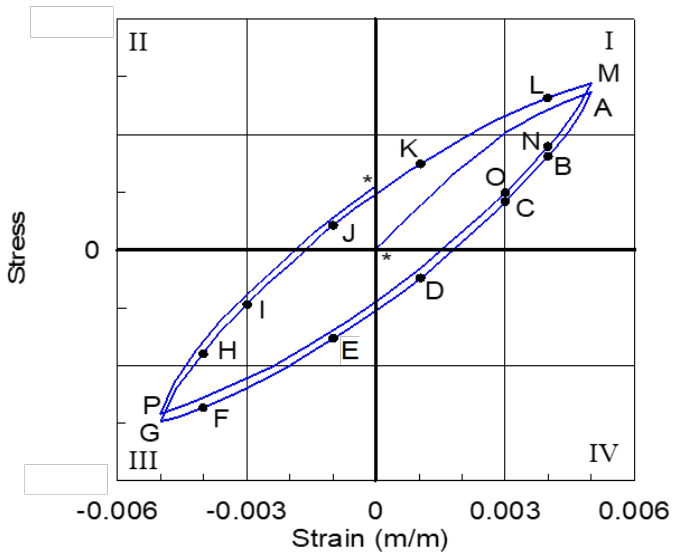

Figure 17.—Schematic of a cyclic load history where interrupted relaxation tests are to be performed at labeled points.

Figure 18 shows the strain-time and stress time response associated with experiment 87-50, along with the stress-strain response for both cycle 1 and 2. It also shows in Figure 18(e) the stress-time response of the 50 uninterrupted fully reversed cycles (UC) that are applied after the two interrupted cycles (IC). Note that points in which a 2-hr hold, relaxation tests, are performed during cycle 1 are labeled B, C, D, E, F, H, I and J wherein the strain values are 0.004, 0.003, 0.001, –0.001, –0.004, –0.003 and –0.001, respectively, see Figure 18(c). In cycle 2 the interruptions were at strain values 0.001, 0.004, 0.004, and 0.003, that correspond to points K, L, N, and O, respectively, see Figure 18(d). Clearly the actual resulting stress-strain response does not match, as expected, the schematic of Figure 17 due to the presence of the various relaxation periods around the loop. This block loading (two interrupted cycles, followed by 50 uninterrupted cycles) was then repeated twice more.

Figure 19 shows a comparison between the interrupted experimental cycles, 1, 53 and 105 and that of the corresponding predicted GVIPS response, while Figure 20 shows the comparison between experiment 87-50 and GVIPS simulation for cycles 2, 54, and 106. The GVIPS model does an overall reasonably good job of predicting the general shape and magnitude of the material response. Although, it generally underpredicts the stress-strain as well as relaxation of stress throughout the cycles, as expected given our previous discussion regarding the difference in material thickness. The GVIPS model also continues to harden between cycles 53 and 100 whereas the experimental response has saturated. From Figure 20 little hardening occurs between cycle 2, 54 and 106 with respect to the experimental response and that of the GVIPS simulation, yet as in Figure 19 the GVIPS model does underpredict the loading response; especially from point P to the origin where it is obvious that GVIPS indicate a state of zero stress while the experiment indicates approximately 62 MPa of stress at zero strain.

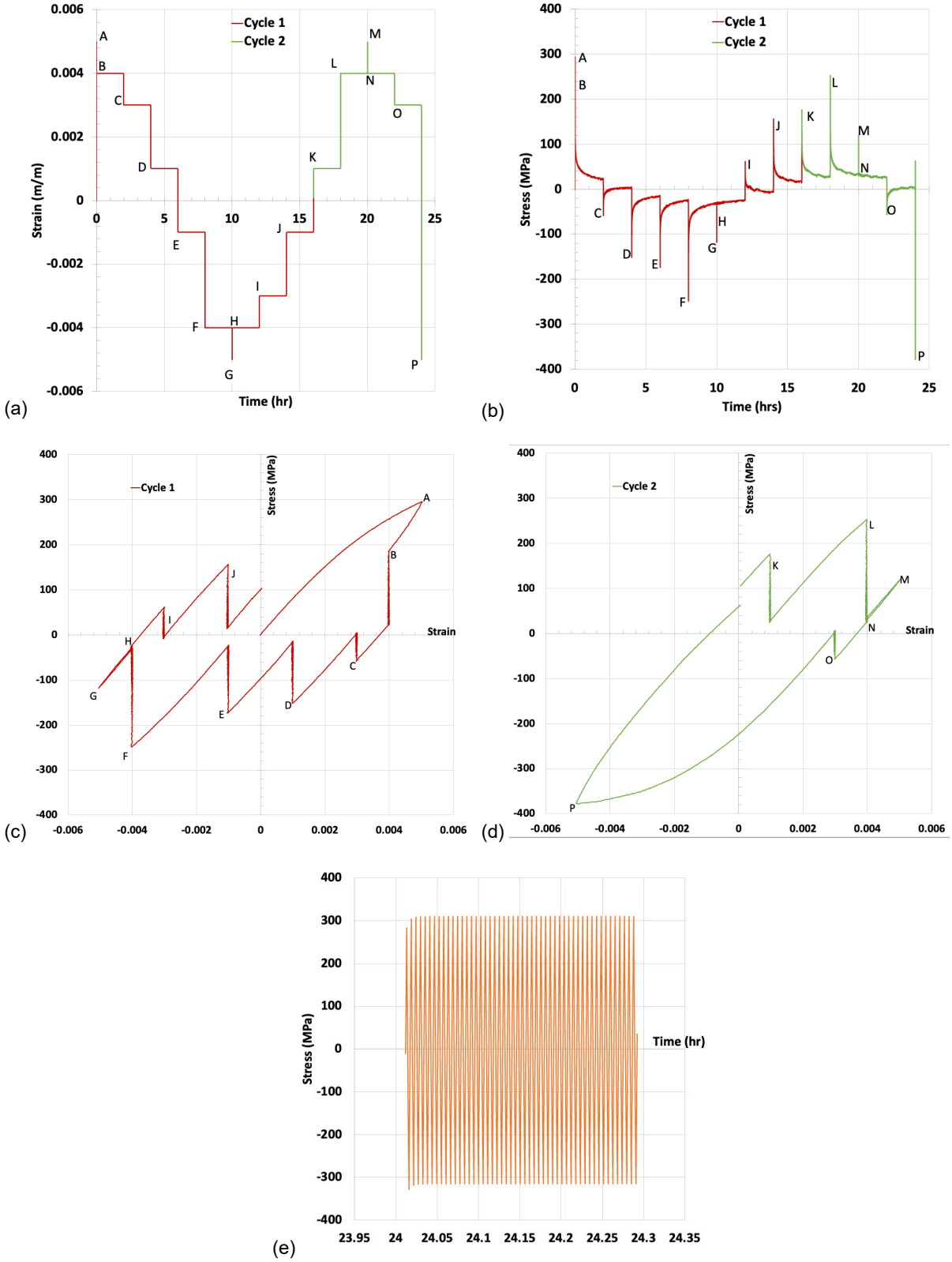

Figure 18.—Description of first two interrupted cycles IC (1 and 2) followed by 50 uninterrupted cycles, UC, associated with test 87-50; (a) strain vs. time, (b) stress vs. time, (c) stress-strain for cycle 1, (d) stress-strain for cycle 2, (e) 50 uninterrupted fully reversed cycles, between 0.005 and –0.005 at 10^{-3} sec^{-1} rate, UC3-UC52.

After application of the previous three block (two interrupted cycles, followed by 50 uninterrupted cycles) loadings three additional blocks of *reversed loading* (Figure 18(c), loaded in compression first, followed by Figure 18(d), loaded in tension first) were applied to the specimen. The resulting response (shown in Figure 21 and Figure 22) are almost a mirror image of that shown in Figure 19 and Figure 20, respectively. The only difference is that the absolute value of the compressive peaks is slightly larger than the associated tensile peaks. Also, the difference (error) between the GVIPS prediction and experimental response for cycles 157 and 209 (see Figure 21) are significantly greater than the first two interrupted cycles 1 and 53 (see Figure 19) thus suggesting that both the number of applied cycles and the effect of load reversal has influenced the evolution of the internal stress greatly and thus the hardening behavior of the model. Note after an additional 50 cycles both the experiment and GVIPS prediction once again indicates shakedown of the material response and predication, see Figure 22. Given the fact that the GVIPS model parameters were characterized using only data in quadrant I and a single fully reversed cycle (using thinner 5-ply specimens) – the overall predictive behavior of the GVIPS model (compared to this thicker material response) is extremely good.

Figure 23 illustrates the relaxation response at Points B and C for experiment 87-50 and the corresponding predicted GVIPS response. As indicated previously and discussed extensively in Arnold and Lerch (2024) examining the relaxation response, particularly in all four quadrants of the stress-strain space and associated state space provide insight into the validity of the functional forms chosen for the hardening ($h(G)$) and thermal recovery ($r(G)$) terms of the model. Clearly in Figure 23(a) each response at Point B, irrespective of the given cycle (i.e., 1, 53 or reversed cycles 157, 209) all follow almost identical relaxation paths experimentally and especially with respect to the GVIPS predictions with the qualitative shape of the curves being in excellent agreement. Although the starting stress levels for the GVIPS predictions for cycles 1 and 53 were different by approximately 3 and 12 MPa, respectively, the final saturation stress was approximately 41 MPa for both. In Figure 23(b), similar qualitative agreement in shape of the relaxation response is observed (once again irrespective of cycle) but this time the saturated stress value is opposite in sign to that of the starting value. As expected, the GVIPS prediction underestimates the starting stress value for cycles 1, 53, 157 and 209 by 60.6, 40.5, 47.6 and 50 percent, respectively and in this case the final saturating stress for the different cycles are slightly different from each other (i.e., approximately 20 percent comparing GVIPS cycle 1 to 53 and 36 percent for cycles 157 compared to 209) as compared to Point B. Examining the remaining stress relaxation response locations, i.e., points D, E, F, H, I, J, K, L, M, N, and O it is clear from Figure 19 to Figure 22 that the functional forms associated with the current GVIPS model adequately represent the TIMETAL 21S material response.

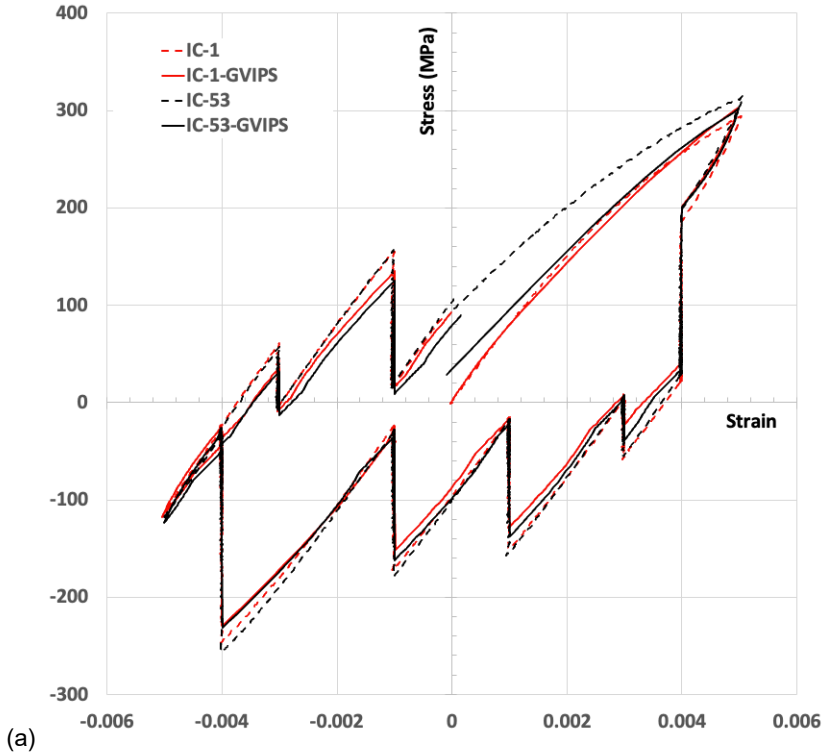

(a)

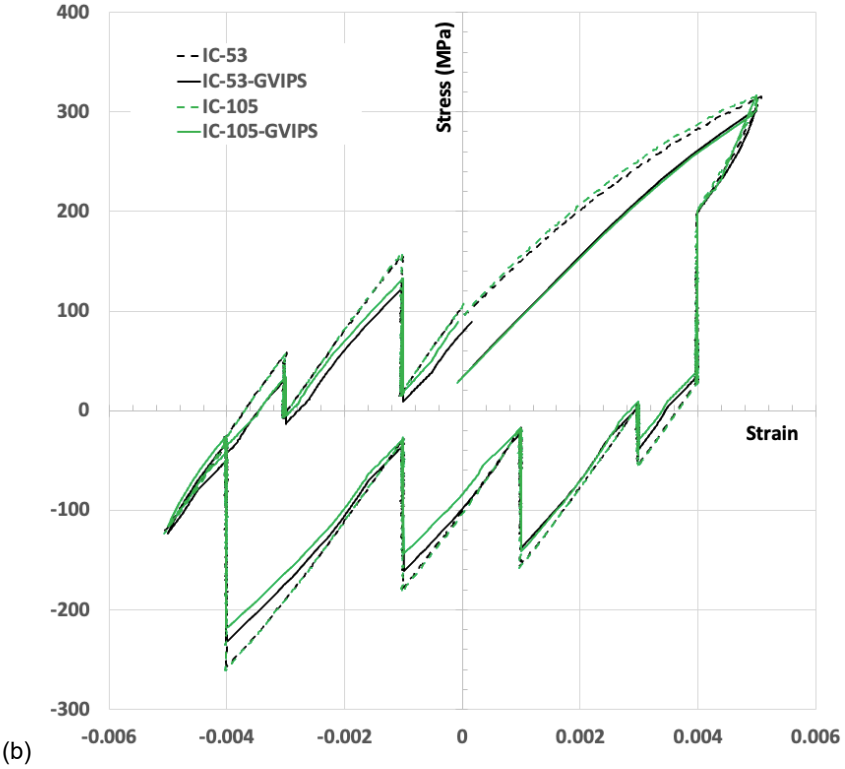

(b)

Figure 19.—Comparison of experiment 87-50 and GVIPS simulation; (a) cycles 1 and 53, (b) cycles 53 and 105.

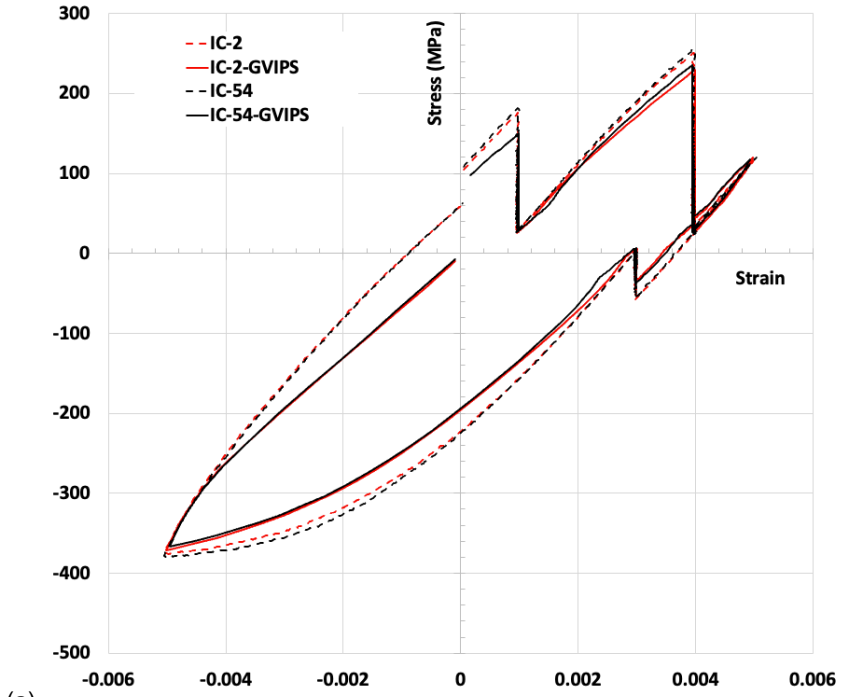

(a)

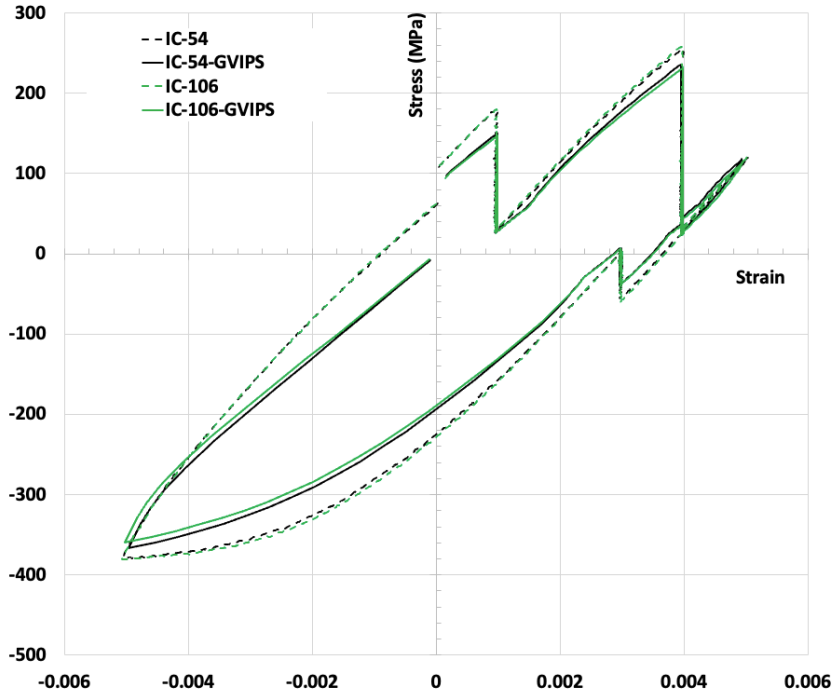

(b)

Figure 20.—Comparison of experiment 87-50 and GVIPS simulation; (a) cycles 2 and 54, (b) cycles 54 and 106.

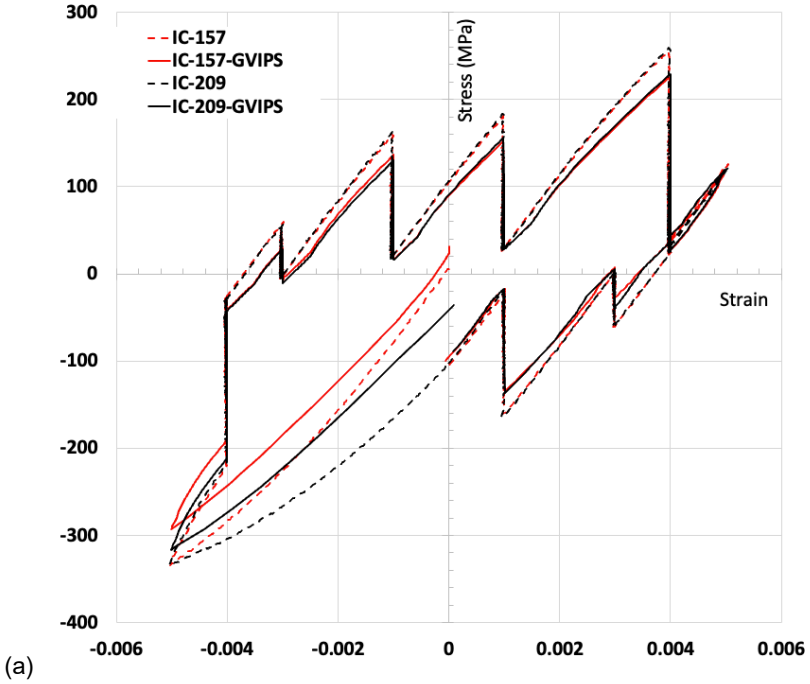

(a)

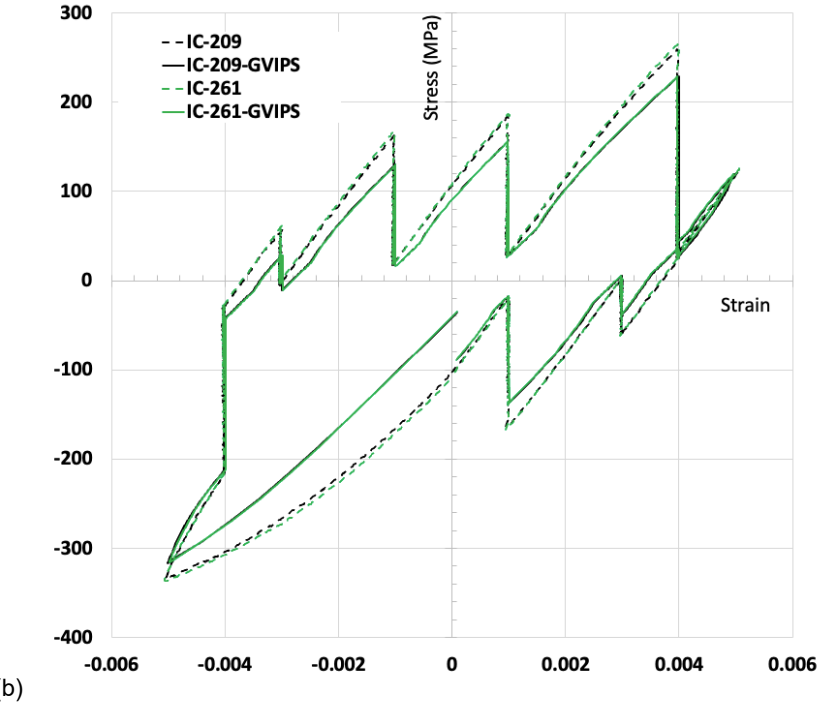

(b)

Figure 21.—Comparison of experiment 87-50 and GVIPS simulation; (a) cycles 157 and 209, (b) cycles 209 and 261.

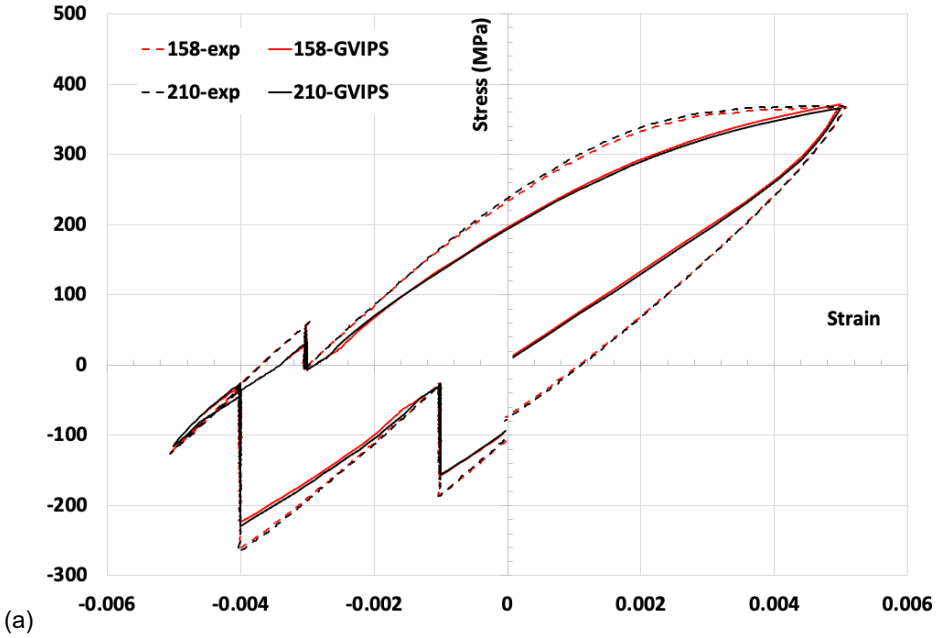

(a)

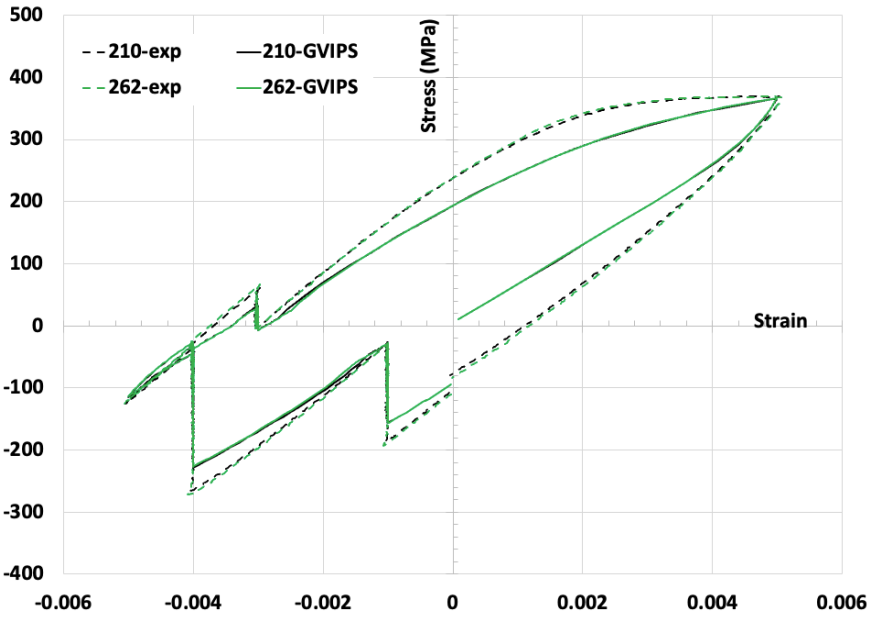

(b)

Figure 22.—Comparison of experiment 87-50 and GVIPS simulation; (a) cycles 158 and 210, (b) cycles 210 and 262.

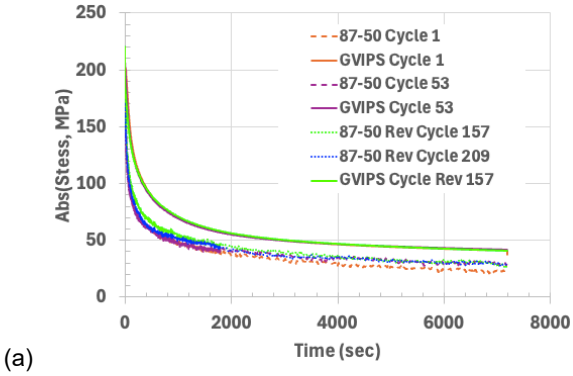

(a)

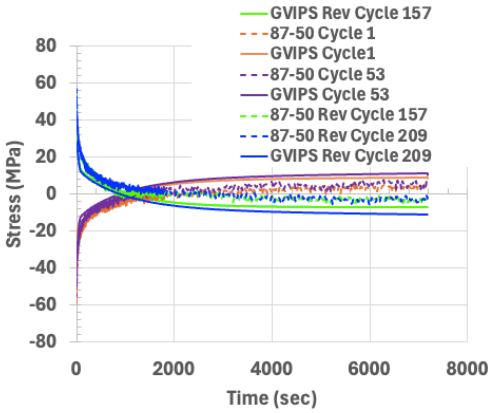

(b)

Figure 23.—Comparison of experiment 87-50 and GVIPS simulation; a) Relaxation response at Point B (see Figure 17(c)) for cycles 1, 53, 157 and 209, and (b) Relaxation response at Point C (see Figure 17(c)) cycles 1, 53, 157 and 209.

The initial stress-strain response associated with experiment 87-21 is shown in Figure 24 along with that of experiment 87-50, the primary difference being that in 87-21 the relaxation response in quadrant I, point B, was skipped as were the relaxation periods in quadrant II as well. Note that the repeatability of the load-up and initial unload path for both experiments match very well as do the relaxation responses at C, D, E (associated with 87-50) and at C′, D′ and E′ (associated with 87-21). The full relaxation response (stress versus time plot) for C and C′ are shown in Figure 25 while those of D, E and D′ and E′ are shown in Figure 26. Note that the initial relaxation in 87-21, point C′, is significantly more rapid than that at point C in 87-50 due to the prior time-dependent deformation that occurred during the strain hold at point B. In contrast the relaxation response of points D and D′ and points E and E′, for both 87-50 and 87-21 respectively, are remarkedly the same. Figure 27 shows the GVIPS simulation response for cycle one of experiment 87-21, where the GVIPS model over predicts the unload path significantly, and thus completely misses the relaxation response at point C′ (i.e., total strain 0.001). However, for subsequent relaxation response predictions (i.e., points D′ and E′) GVIPS does a very good job of replicating the experimental response. Comparison of the full relaxation response for point D′ of 87-21 and GVIPS prediction is shown in Figure 28. Clearly, the shape of the curve is qualitatively captured nicely, with the initial reduction in stress being underpredicted by the current characterization of the GVIPS model. The additional cyclic and relaxation responses for experiment 87-21 were not simulated since it was found that the subsequent test histories were done sequentially on different days with rezeroing of stress and strain taking place at the beginning of each test thus rendering it impossible to discern the initial internal state of the material for each subsequent block loading, see Lissenden et al., 2007.

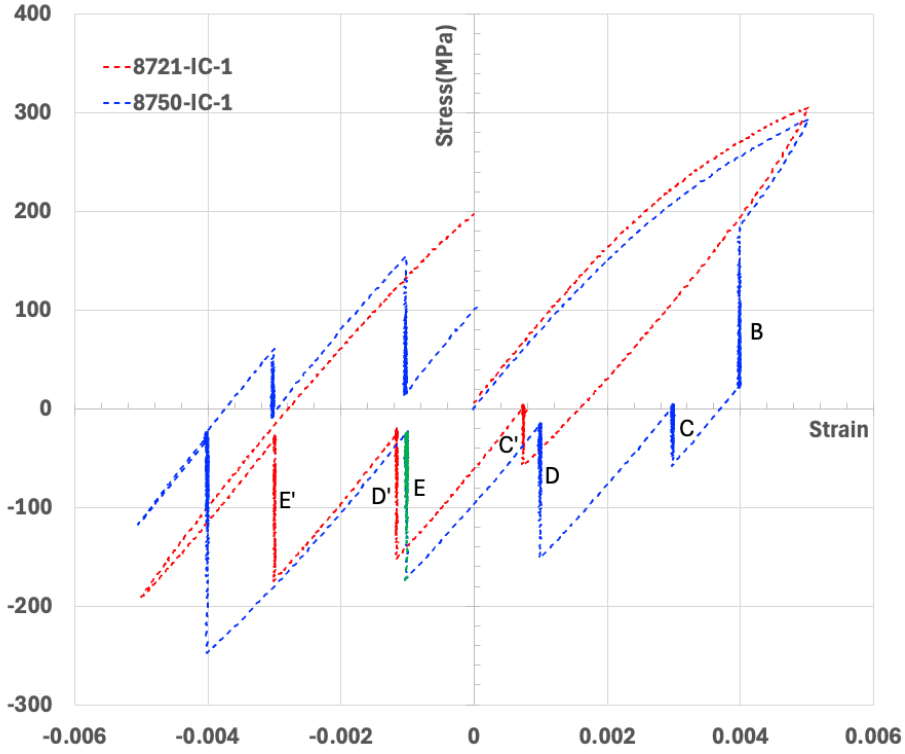

Figure 24.—Comparison of the first interrupted cycle of experiments 87-21 and 87-50.

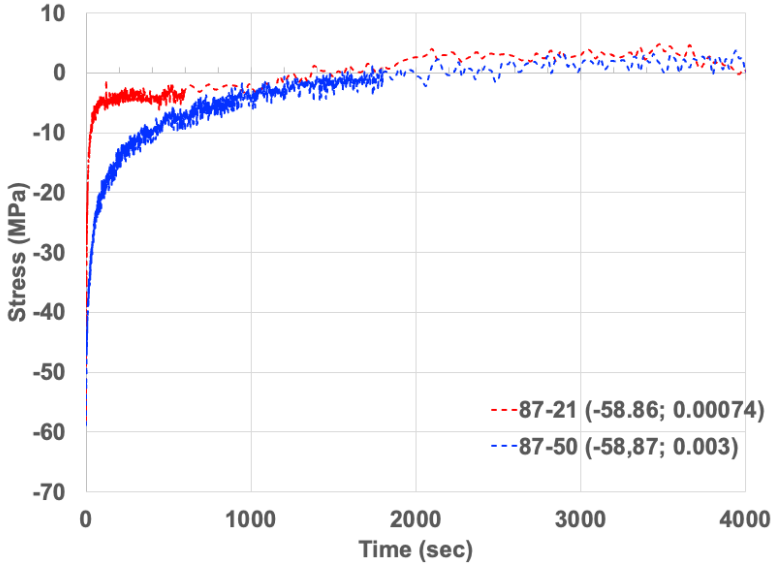

Figure 25.—Comparison of experimental relaxation response at points C (87-50) and C′ (87-21), see Figure 24.

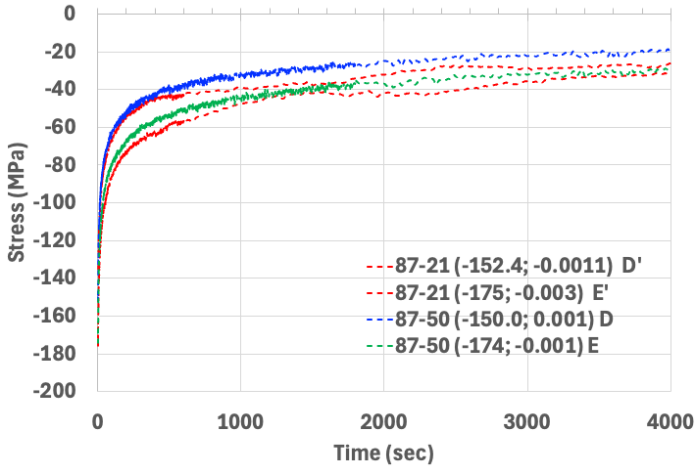

Figure 26.—Comparison of experimental relaxation response at points D and E (87-50) and D′ and E′ (87-21), see Figure 24.

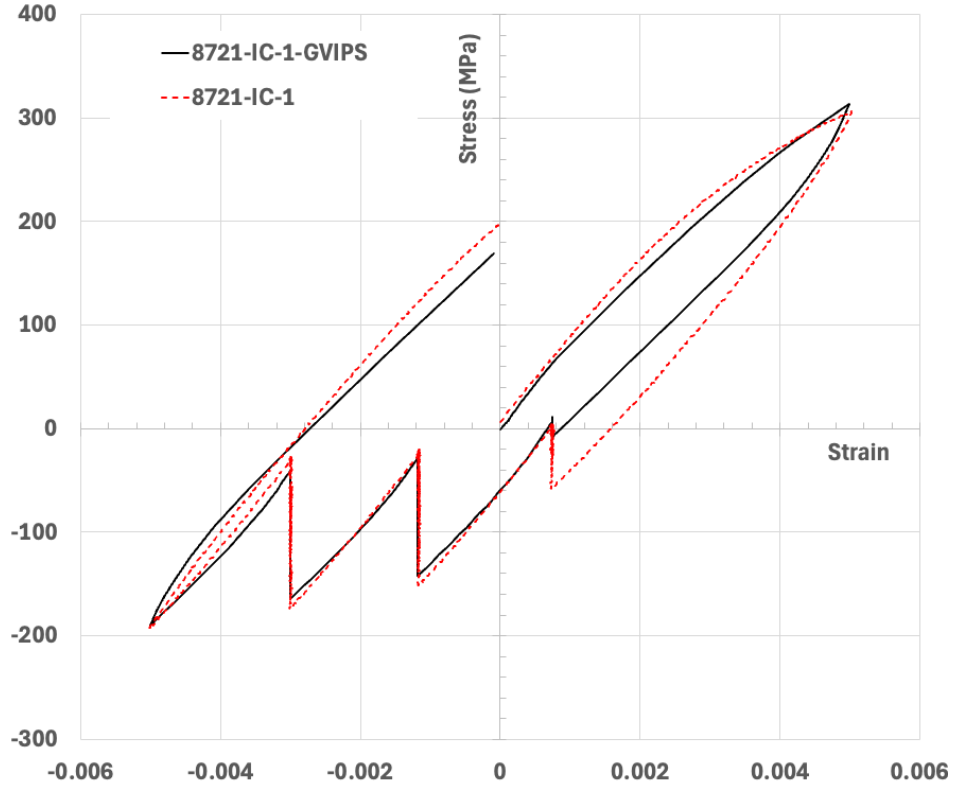

Figure 27.—Comparison of the first interrupted cycle of experiments 87-21 and the associated GVIPS prediction.

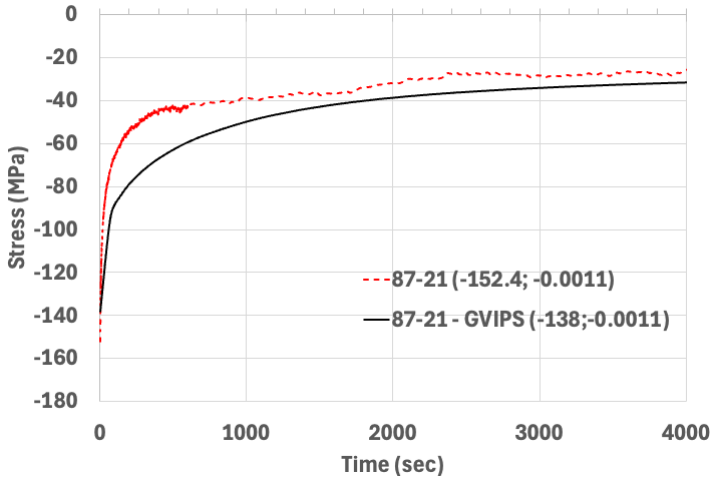

Figure 28.—Comparison of experimental relaxation response at point D′ (87-21), see Figure 24, and associated GVIPS prediction.

Numerical Implementation

All the numerical simulations discuss herein were carried out utilizing the commercial Finite Element (FE) software ABAQUS, wherein the GVIPS model was implemented via the ABAQUS's user material subroutine (UMAT). This UMAT (see Appendix A) contains the multimechanism GVIPS model (i.e., flow and evolutionary laws) and implicit backward Euler integration method (see Saleeb and Wilt, 1993, Saleeb et al., 1998 and 2000) due to its unconditional stability and robustness. The standard ABAQUS solver with automatic incrementation was utilized to run all cases to completion. All simulations were performed given a single conventional three-dimensional solid element in ABAQUS (C3D8). Application of reduced versus full integration did not demonstrate any benefit given only a single element. The constitutive model parameters used for all simulations (GVIPS) were characterized as described in the Model Characterization section. Application of simple loading cases (e.g., tension, creep, relaxation, and simple strain-controlled (Mode I) or stress-controlled (Mode II) cyclic loading) was straightforward based on the corresponding control mode. For a strain-controlled mode, the specified strain (displacement in a single unit-length element) was applied directly with a time-based amplitude definition in ABAQUS. Results for simple Mode-I loadings are shown in Figure 5 to Figure 8. For a stress-controlled mode, the specified stress (nodal force in a single unit-length element) was also applied with a smooth time-based amplitude function to minimize numerical disruptions. The resultant cyclic stress-strain responses are demonstrated in Figure 10 to Figure 11, and Figure 13. The simulation time for cyclic load cases ranged between 48 to 256 sec depending upon the number of applied cycles. While setting lower fixed incrementations might help obtain a smoother stress-strain curve, the simulation time required will become much longer- especially for loading cases with hundreds of cycles. Therefore, incrementations were set within ABAQUS to be automatic to optimize convergence and simulation time.

Implementation of the complex interrupted loading cases (e.g., Figure 18 to Figure 21) required the development of a script to facilitate automatic writing of the complex cycles into the corresponding ABAQUS input deck. All complex loading cases were strain-controlled (Mode-I), which helped with automating the process. Every strain-controlled ABAQUS loading cycle requires a Step definition with initial (start) step time, total (end) step time, min step increment, and max step increment. In order to implement multiple cycles with varying start/end strain points, the script utilizes the loading data file generated by the experimentalist (.dat file) to create the required steps with the specified time requirements (written in .inp format for ABAQUS use, see Appendix B). The simulation time for

complex interrupted loading cases ranged from 210 to 355 sec depending on the number of cycles applied. All simple and complex loading cases ran to completion without any major issues, which demonstrates the numerical robustness of the fully associative, potential-based (GVIPS) constitutive model. The state dependent variables (SDVs) tracking back stress and total stress components can be extracted from the output database (Odb) file in ABAQUS to gain a better understanding of the internal variables as needed.

Conclusions

Hereditary behavior encompasses such important features as nonlinearity, loading-rate sensitivity, creep, relaxation, creep-plasticity interaction effects as well as memory effects for both the short-term (transient) and long-term (steady states of limit equilibrium) material responses such as cyclic ratcheting and/or shakedown. To date a general, potential-based, viscoelastoplastic multimechanism deformation model known as GVIPS has been formulated, implemented and characterized for the titanium alloy, TIMETAL 21S. In this study, the predictive ability of a six-mechanism viscoelastic and three-mechanism viscoplastic model with a saturating material hardening function was evaluated relative to its ability to predict cyclic behavior under different loading conditions (i.e., strain-control and stress-control) and complex interrupted cyclic behavior with multiple 2-hr relaxation hold periods at 650 °C. The material characterization of TIMETAL 21S, was accomplished using the *COMPARE* software, a fully automated procedure for material parameter estimation, and a fairly comprehensive set of test data under different loading conditions, i.e., tensile tests at 3 different loading strain rates, several creep and relaxation tests and a single fully reversed, strain-controlled cyclic test.

The overall performance of the multimechanism GVIPS model with saturating hardening function was found to be *very capable* of predicting the cyclic response under both strain-control and stress-control at varying rates of loading, particularly given the fact that only a single fully reversed cycle along with monotonic loading (i.e., tensile, creep and relaxation tests) all within quadrant I of the stress-strain space was used for characterization. It was particularly interesting that the model was capable of reasonably capturing the rate of accumulated strain during ratchetting under tensile mean stress. The model clearly was able to predict the additional strain accumulation caused by cycling over that which would be produced from merely the inelastic strain accumulation caused by monotonic creeping at the mean tensile response. Given complex interrupted cyclic response, the model was able to both qualitatively and even quantitatively predict reasonably well both the cyclic and associated relaxation periods (in all quadrants of the stress-strain space) thus confirming the validity of the chosen functional forms for both hardening and thermal recovery. The quantitative inaccuracy being associated with the fact that the material specimens tested by Lissenden et al., 2007, was significantly “softer” than that tested by Castelli reported in Saleeb et al., 1994, which was used for characterization of the model parameters. Consequently, a recalibration of the GVIPS model parameters will be conducted in the future using a finite set of Lissenden tests (e.g., strain-controlled, fully reversed, tests 87-4 and 87-41) for characterization while reserving both stress and mixed controlled tests for validation of the predictive ability of the GVIPS model.

Finally, this study demonstrated the predictive ability of the GVIPS model to accurately represent the complex cyclic response of TIMETAL 21S at elevated temperature (i.e., 650 °C), particularly given the limited amount of characterization data utilized. Further, it reinforces the need for an analysist to understand not only the theoretical underpinning of a given constitutive model but also how that model’s material parameters have been characterized before blindly utilizing it to predict the behavior of a given specimen or application composed of the same material (i.e., idealization consistency).

Appendix A.—UMAT Routine

```
c%%%%%%%%%%%%%%%%%%%%%%%%%%%%%%%%%%%%%%%%%%%%%%%%%%%%%%%%%%%%%%%%%%%%%%%%%%
c  This is the latest and greatest version of
C       GVIPS - 2024 updated to include saturated form in IJP 2004 (or Comp B)
C
C    Saleeb, A.F., Arnold, S.M., Castelli, M.G, Wilt, T.E., and Graf, W.E., "A General
C     Hereditary Multimechanism-Based Deformation Model With Application
C     to The Viscoelastoplastic Response of Titanium Alloys, Int. Jnl. Of Plasticity,
C     Vol. 17, No. 10, pp. 1305-1350. Oct. 2001
C
C    Saleeb, A.F. and Arnold, S.M. ; "Specific Hardening Function
C    Definition and Characterization of A Multimechanism Generalized Potential-Based
C    Viscoelastoplasticity Model", Int. Jnl  of Plasticity, Vol. 20, pp. 2111-2142,2004.
C
C    and
C
C    Saleeb, A.F., Wilt, T.E., and Al-Zoubi, N:  "An Anisotropic Viscoplastic
C     Model for Composites – Sensitivity Analysis and Parameter Estimation",
C     Composite Part B: Engineering, Vol. 34,No.1, pp 21-39, 2003
C
C    Saleeb, A.F., Gendy, A.S., T.E. Wilt; "Parameter-Estimation Algorithms
C     For Characterizing A Class of Isotropic and Anisotropic Viscoplastic Material
C     Models", Int.  Jnl. of the  Mechanics of Time Dependent Materials ,Vol. 6, No.4,
C      pp 323-361, 2002.
C
C ==================================================================
C      This code was prepared by Drs. S.M. Arnold and A.F. Saleeb
C        Code is considered proprietary to NASA GRC
C.        To execute UMAT requires IMPL8 library, see https://software.nasa.gov/
C.  Copyright 2024 United States Government as represented by the Administrator of the
C.   National Aeronautics and Space Administration. No copyright is claimed in the
C.   United States under Title 17, U.S. Code. All Other Rights Reserved.
C
C ==================================================================
c%%%%%%%%%%%%%%%%%%%%%%%%%%%%%%%%%%%%%%%%%%%%%%%%%%%%%%%%%%%%%%%%%%%%%%%%%%
      subroutine umat(stress, statev, ddsdde, sse, spd, scd,
     &              rpl, ddsddt, drplde, drpldt,
     &              stran, dstran, time, dtime, temp, dtemp, predef, dpred,
     &              cmname, ndi, nshr, ntens, nstatv, props, nprops, coords,
     &              drot, pnewdt, celent, dfgrdo, dfgrd1, noel, npt, layer,
     &              kspt, kstep, kinc)
c   Purpose: Drives the calculation of Inelastic Strain and back stress evolution
c     INPUT:
c       stran   - current total strain at beginning of increment
c       dstran  - current strain increment
```

```
c       time(1) - time step at beginning of inc.
c       time(2) - current total time at beginning of inc.
c       dtime   - time increment
c       temp    - temperature at beginning of inc.
c       dtemp   - temperature inc.
c       noel    - element #
c       npt     - int. point #
c       kstep   - step #
c       kinc    - increment #

c     OUTPUT:
c       ddsdde  - jacobian matrix
c       stress  - stress at end of increment
c       statev  - state variables

c     INCLUDE 'ABA_PARAM.INC'
      implicit real*8 (a-h,o-z)
      parameter (nprecd=2)

      character*8 cmname

      common /kio/ nio,nplvl

      dimension stress(ntens),statev(nstatv),ddsdde(ntens,ntens),
     &          ddsddt(ntens),drplde(ntens),stran(ntens),dstran(ntens),
     &          time(2),predef(1),pred(1),props(nprops),coords(3),
     &          drot(3,3),dfgrdo(3,3),dfgrd1(3,3)

      dimension ANLVAR2(300)

      nio = 6

      write(nio,*) 'here'
c     if(noel.eq.1 .and. npt.eq.1) then
c       NPLVL = 10
c     else
      NPLVL = 1
c     endif
c      NPLVL = 0


      IF(NPLVL.EQ.1) THEN
      write(6,*) ' ////////////////////////////////////////////////////'
      write(6,*) ' kstep ',kstep,' kinc ',kinc
      write(6,*) ' TIME ',time(1), ' dtime ',dtime
c     write(6,*) ' umat stran ',(stran(ii),ii=1,6)
```

```
c     write(6,*) ' umat dstran ',(dstran(ii),ii=1,6)
c     write(6,*) ' umat nstatv ',nstatv
c     write(6,*) ' umat nprops ',nprops
c     write(6,*) ' umat props ',(props(ii),ii=1,nprops)
      write(6,*) ' call m11stn'
      ENDIF

      CALL M11STN(TIME,PNEWDT,
     &          STRESS,STATEV,STRAN,DSTRAN,DTIME,DDSDDE,
     &          PROPS,NPROPS,
     &          KSTEP,KINC,NOEL,NPT,NSTATV)

      write(6,*) ' kstep ',kstep,' kinc ',kinc

      RETURN
      END
c%%%%%%%%%%%%%%%%%%%%%%%%%%%%%%%%%%%%%%%%%%%%%%%%%%%%%%%%%c
      SUBROUTINE M11STN(TIME,PNEWDT,
     &               STRESS,STATEV,STRAN,GDELPS,DT,D,
     &               PROPS,NPROPS,
     &               KSTEP,KINC,NOEL,NPT,NSTATV)

c     purpose:  calculate current stress state and current
c           tangent stiffness using a backward euler
c           integration scheme


      IMPLICIT DOUBLE PRECISION (A-H,O-Z)

      common /kflow/ iflow, ievo

      common /kio/ nio,nplvl
      COMMON /KMODS/ Y(500),YOLD(500)
      COMMON /KVELAS/ ES,PR,EM(30),RHO(30),NEL
      COMMON /KVESG2/ SIGMO(6,30),SIGM(6,30),EEPS(6),DSIGM(6,50,30)
      COMMON /KVESG3/ SIGMde(6,30)
      COMMON /KVEVPC/ ANLVAR2(300),YTMP(20)
      COMMON /KVISC/ NVP
      COMMON /KZOROI/ INCO,INCC,ICOUNT(8)

      DIMENSION STRESS(6),STRAN(6),GDELPS(6),D(6,6),STATEV(NSTATV)
      DIMENSION PROPS(NPROPS)
c
c  Note: Material parameters Es, nu, NEL(Em,rho)  : 3 + 5NVP + psi + zeta, + 4 stiffness damage
c         + 4NVP strength reduction parameters + 2 cutoff values = 11 + 9NVP
c   -------  order of these parameters is not as written here see IMPL8 for order -----
```

```
c  ------------------------------------------------------------
c  number of viscoelastic constants:  nel   reversible mechanisms
c  number of viscoplastic constants:  nvp   irreversible mechanisms
c
c ---- order of storage of constants in anlvar
c
c      Nel, Nvp, Es, nu, [(Em1, rho1), …,( EmNel, rhoNel)],
c      kappaf, [kappa_1, …, kappaNvp],  n, mu, [m1, …, mNvp], [beta1, …, betaNvp],
c      [R1, …, RNvp], [H1, …, HNvp], [Cb1, …, CbNvp], [Y01, …, YoNvp],
c      [mud1, …, mud Nvp], [nd1, …, nd Nvp], Cs, Yso, musd, nsd, eta, squig, epsIcut, epsecut
c
c  where nsd is the space dimension:  3D = 6 ,  2D=3

      ntot = (2 + 2*props(1)) + (11 + 9*props(2))

      nel = props(1)
      nvp = props(2)
      do 1 i=1,ntot
        anlvar2(i) = props(i+2)
 1    continue

      if(kstep.eq.1 .and. kinc.eq.0) then
        write(6,*) 'STN  anlvar2 * ',(anlvar2(ii),ii=1,ntot)
      endif

c      if(npt .eq. 1) then
c        write(nio,*) '  ENTER STN NOW '
c        write(nio,*) 'stn:  NPT ',npt
c        write(nio,*) 'stn:  kstep ',kstep,' icount ',icount(npt)
c        write(nio,*) 'stn:   dt ',dt
c      endif

c-------------------------------------------------------------
c  at beginning of time step
c  initialize damage variable, theta
c-------------------------------------------------------------
      NN=6
      IF(KINC.EQ.1 .OR. KINC.EQ.0) THEN
        IF(KSTEP .EQ. 1) THEN
c-------------------------------------------------------------
c  initialize damage variable, theta
c-------------------------------------------------------------
          DO I=1,NVP
            STATEV((NVP*NN + NEL*NN) + NN + I) = 1.0
          END DO
c ---------------------------------------------
```

```
c  initialize elastic damage variable, psi
c-------------------------------------------
        STATEV((NVP*NN+NEL*NN)+NN + 2*NVP + 1) = 1.0

       ENDIF
      ENDIF

c-------------------------------------------------------------
c  update yold (state variable) vector:  time= t_n
c  note that statev dimension must be 500 in input file
c-------------------------------------------

      DO 30 I = 1,500
        YOLD(I) = STATEV(I)
 30   CONTINUE

c-------------------------------------------------------------
c  call implicit integrator
c------ Call IMPL8 - which does the calculating of the flow and evolutionary laws -
c-------------------------------------------------------------
c
      if(nplvl.eq.1) write(6,*) ' stn:  call impl8 time ',time
      CALL IMPL8(TIME,DT,PNEWDT,GDELPS,D,NOEL,NPT,KSTEP,KINC)
      if(nplvl.eq.1) write(6,*) ' stn:  return impl8'
c-------------------------------------------------------------
c  return implicit integrator
c-------------------------------------------------------------
c-------------------------------------------------------------
c  update state variable (statev) vector:  time= t_n+1
c
c-------------------------------------------------------------

      DO 35 I = 1,500
        STATEV(I) = Y(I)
 35   CONTINUE

c      if(npt.eq.1) then
c        write(6,*) ' statev 9 ',statev(9)
c      endif

c-------------------------------------------------------------
c  copy updated stress to ABAQUS STRESS array
c-------------------------------------------------------------

      DO 40 I = 1,6
        STRESS(I) = STATEV(I)
```

```
 40   CONTINUE

      if(nplvl.eq.1) then
      write(6,*) ' NPT ',npt
      write(6,*) ' STN: STRESS ',(stress(ii),ii=1,6)
      endif

      RETURN
END
```

Appendix B.—ABAQUS Tensile Input Deck

```
*HEADING
 single element - Ti-Metal-21s
*NODE
 1, 0.0, 0.0, 0.0
 2, 1.0, 0.0, 0.0
 3, 1.0, 1.0, 0.0
 4, 0.0, 1.0, 0.0
 5, 0.0, 0.0, 1.0
 6, 1.0, 0.0, 1.0
 7, 1.0, 1.0, 1.0
 8, 0.0, 1.0, 1.0
***ELEMENT,TYPE=C3D8
*NSET, NSET=TOP
3,4,7,8
*NSET, NSET=right
2,3,6,7
*NSET, NSET=left
1,4,5,8
*NSET, NSET=front
5,6,7,8
*NSET, NSET=back
1,2,3,4
*NSET, NSET=bottom
1,2,5,6
*NSET,NSET=ALL
1,2,3,4,5,6,7,8
*ELEMENT,TYPE=C3D8RH, ELSET=BLOCK
  1,1,2,3,4,5,6,7,8
*SOLID SECTION, ELSET=BLOCK, MATERIAL=ISO
          1.,
*HOURGLASS STIFFNESS
 165
*MATERIAL, NAME=ISO
**ELASTIC
** 0.4226E7, 0.3
**Ti-Metal-21s; 6 viscoelastic and 3 viscoplastic mechanics with stiffness
and strength reduction
*User Material, constants=54
**N_Vi,   N_vp,       Es,       nu,       Em_1,   rho_1,     Em_2,   rho_2
   6.,      3.,   21.733E9,   0.365,   41.37E9,    0.5,    6.895E9,    50.
**Em_3,   rho_3,     Em_4,      rho_4,    Em_5,   rho_5,    Em_6,    rho_6
 21.12E9,  974.,  6.523E9,    9693.,    3.965E9,  14460.,  3.434E9,  28218.
**Kappa,   kappa_1,  kappa_2,  Kappa_3,   n,      mu,       m1,      m2,
  4.25E6,  57.0e6,   56.9e6,   43.5e6,  1.01646,  2.21264e14, 1.0,  4.02489
**m3,   Beta_1,     Beta_2,    Beta_3,  R1,       R2,          R3,      H1,
7.21429,   1.0,    6.64696,    4.5,    0.6045, 1.5483E-7,  1.7506e-2, 19000e9
** H2,    H3,   cd_1,      cd_2,     cd_3,    Yd_1,     Yd_2,     Yd_3,
```

```
3.11e9,  1.42e9,  1.09631, 24.2601, 7.44875, 8.16947E-005, 0.000443603,
0.000100625
**mu_d_1,  mu_d_2,   mu_d_3,   nd_1,  nd_2,    nd_3, c_e,     Y_e,
1.12356E+008, 46.664,  1590.87,   1.0, 1.0,    1.0,  1.0,     1.0
**mu_e,    n_e,    zeta_e, xeta, epsIcut, epsEcut
1.0,      1.0,      0.0,    0.0,  0.99999,  0.99999
**
*DEPVAR
 500
**
**
*BOUNDARY
bottom,2
left,1
back,3
**right,1
**front,3
**
*AMPLITUDE,NAME=TENSILE
0,0.0, 12,0.01, 60, 0.05
*************
*STEP, INC=100000
*STATIC
 0.1,60.0,1e-8,1.0
*CONTROLS, PARAMETERS=TIME INCREMENTATION
,,,,,,,20
***************
*BOUNDARY, AMPLITUDE=TENSILE,OP=MOD
  TOP,2,,1
********
*OUTPUT, HISTORY, FREQUENCY=1
*ELEMENT OUTPUT,ELSET=BLOCK
S22,S11,S33
SDV
*OUTPUT,FIELD, FREQUENCY=1
*NODE OUTPUT,NSET=ALL
U
*NODE OUTPUT,NSET=ALL
RF
*NODE PRINT, FREQUENCY=1
RF
*OUTPUT, HISTORY, FREQUENCY=1
*EL PRINT,  FREQUENCY=1
S
E
SDV
*RESTART,WRITE,FREQUENCY=1
*END STEP
```

References

Arnold, S.M. and Lerch, B., 2024, "Data Content Necessary to Support Development, Characterization, and Validation of Thermomechanical Constitutive Models: Deformation and Damage," NASA/TP-20240001190.

Arnold, S. M., Saleeb, A.F., and Castelli M.G., 1994a, A Fully Associative, Non-linear Kinematic, Unified Viscoplastic Model for Titanium-based Matrices, Life Prediction Methodology for Titanium Matrix Composite, ASTM STP 1253, W.S. Johnson, J.M. Larsen, and B.N. Cox, Eds. American Society for Testing and Materials, Philadelphia, pp. 231-256, or NASA TM-106609.

Arnold, S.M.; and Saleeb, A.F., 1994, On the Thermodynamic Framework of Generalized Coupled Thermoelastic Viscoplastic - Damage Modeling. Int. J. Plasticity, 10, 263-278.

Arnold, S.M.; Saleeb, A.F., and Castelli, M.G., 1994b, A Fully Associative, Nonisothermal, Nonlinear Kinematic, Unified Viscoplastic Model for Titanium Based Matrices, Thermomechanical Fatigue Behavior of Materials: Second Volume, ASTM STP 1263, M.J. Verrilli and M.G. Castelli, Eds., Philadelphia, or NASA TM-106926.

Arnold, S.M., Saleeb, A.F, and Wilt, T.E., 1995, A Modeling Investigation of Thermal and Strain Induced Recovery and Nonlinear Hardening in Potential Based Viscoplasticity. J. Eng. Mater. Technol. ASME 117, 157-167.

Arnold, S.M., Saleeb, A.F. and Castelli, M.G., 2001, A General Time Dependent Constitutive Model: Part II: Application to A Titanium Alloy. J. Eng. Mater. Technol. ASME 123, 65-73, see also NASA TM-1997-107494.

Baig, M., Owusu-Danquah, J., Campbell, A.A., Duffy, S.F., 2023, Review: Inelastic Constitutive Modeling: Polycrystalline Materials. Materials, 16, 3564.

Chaboche, J.L., 2008, A Review of Some Plasticity and Viscoplasticity Constitutive Theories, Int. J. Plasticity 24, 1642-1693.

Chaboche, J.L., 1989, Constitutive Equations for Cyclic Viscoplasticity. Int. J. Plasticity 5, 247-302.

Coleman., B.D. and Gurtin, M.E., Thermodynamics with Internal "State Variables". J. Chem. Phys. 47, 597-613.

Freed, A.D. and Walker, K.P., 1993, Viscoplasticity with Creep and Plasticity Bounds. Int. J. Plasticity 9, 213-242.

Hart, E.W., 1976, Constitutive Relations for Nonelastic Deformation of Metals, J. Eng. Mater. Technol. ASME 98, 193-202.

Horstemeyer, M.F. and Barnmann, D.J., 2010, Historical Review of Internal State Variable Theory for Inelasticity, Int J. Plasticity, 26, 1310-1334.

Hübel, H., 1996, Basic conditions for material and structural ratcheting. Nucl. Eng. Des. 162, 55–65.

Hui, C.Y., 1985, A Uniformly Valid Asymptotic Solution of Hart's Equations for Constant Inelastic Extensional Strain Rate. Int. J. Solids and Struct. 21, 411-421.

Krausz, A.S. and Krausz, K., (eds.), 1996, Unified Constitutive Laws of Plastic Deformation. Academic Press, New York.

Krempl, E., 1996, A Small Strain Viscoplasticity Theory Based on Overstress, In: Unified Constitutive Laws of Plastic Deformation, Krausz, A and Krausz, K. (Eds.), Academic, San Diego, pp. 281-318.

Kumar, V., Morjaria, M. and Mukherjee, S., 1980, Numerical Integration of Some Stiff Constitutive Models of Inelastic Deformation, J. Eng. Mater. Technol. ASME 102, 92-96.

Lemaitre, J.; and Chaboche, J.L., 1990, Mechanics of Solid Materials. Cambridge University Press, New York.

Lissenden, C.J., Doraiswamy, D., and Arnold, S.M., 2007, Experimental Investigation of Cyclic and Time-Dependent Deformation of Titanium Alloy at Elevated Temperature, Int. J. Plasticity 23, 1-24.

Lubliner, J., 1973, On the Structure of Rate Equations of Materials with Internal Variables. Acta Mech. 17, 109-119.

Robinson, D.N., 1987, A Unified Creep-Plasticity Model for Structural Metals at High Temperatures. ORNL TM-5969.

Saleeb, A.F. and Arnold, S.M., 2004, Specific hardening function definition and characterization of a multimechanism generalized potential-based viscoelastoplasticity model, Int. J. Plasticity 20, 2111-2142.

Saleeb, A.F. and Arnold, S.M., 2001, A General Reversible Hereditary Constitutive Model: Part I: Theoretical Developments, J. Eng. Mater. Technol., ASME 123, 51-64, see also NASA TM-1997-107493.

Saleeb, A.F. and Wilt, T.E., 1993, Analysis of the Anisotropic Viscoplastic-Damage Response of Composite Laminates-Continuum Basis and Computational Algorithms," Int. J. Num. Meth. Eng. 36, 1629-1660.

Saleeb, A.F., Wilt, T.E., and Li, W. (1998): "An Implicit Integration Scheme for Generalized Viscoplasticity with Dynamic Recovery," Comp. Mech., Vol. 21, No. 6, pp. 429-440

Saleeb, A.F., Wilt, T.E., and Li, W, (2000): "Robust Integration Schemes for Generalized Viscoplasticity with Internal-State Variables," Int. J. Comput. & Struct, Vol. 74, pp. 601-628.

Saleeb, A.F., Arnold, S.M., Castelli, M.G., Wilt, T.E., and Graf, W.E., 2001, A General Hereditary Multimechanism-Based Deformation Model With Application to The Viscoelastoplastic Response of Titanium Alloys. Int. J. Plasticity 17, 1305-1350.

Saleeb, A.F., Wilt, T.E., Trowbridge, D.A., and Gendy, A.S., 2002, Effective Strategy for Automated Characterization in Complex Viscoelastoplastic and Damage Modeling for Isotropic/Anisotropic Aerospace Materials, J Aerospace Eng. 15, 84-96.

Saleeb, A.F., Wilt, T.E., Al-Zoubi, N.R. and Gendy, A.R., 2003, An Anisotropic Viscoelastoplastic Model for Composites – Sensitivity Analysis and Parameter Estimation, Composites: Part B, 34, 21-39.